FINAL REPORT

"MEMS RF Switches with Ultra-High Switching Speeds"

Report Date: May 25, 2001

Report Period: June 1, 2000 through February 1, 2001

Sponsored by

Defense Advanced Research Projects Agency (DoD)
Weapons Sciences Directorate, AMRDEC

ARPA Order D611/73

Issued by U.S. Army Aviation and Missile Command Under

Contract No. DAAH01-00-C-R146

Effective Date of Contract: June 1, 2000

Expiration Date of Contract: February 1, 2001

Principal Investigator: Dr. Frank T. Djuth

Geospace Research, Inc.

550 N. Continental Blvd., Suite 110
El Segundo, CA 90245

Voice: (310) 322-1160
FAX: (310) 322-2596
E-Mail: djuth@ix.netcom.com

20010604 089

REPORT DOCUMENTATION PAGE

Public reporting burden for this collection of information is estimated to average 1 hour per response, including the time for reviewing instructions, searching existing data sources, gathering and maintaining the data needed, and completing and reviewing the collection of information. Send comments regarding this burden estimate or any other aspect of this collection of information, including suggestions for reducing this burden, to Washington Headquarters Services, Directorate for Information Operations and Reports, 1215 Jefferson Davis Highway, Suite 1204, Arlington, VA 22202-4302, and to the Office of Management and Budget, Paperwork Reduction Project (0704-0188), Washington, DC 20503.

1. AGENCY USE ONLY (Leave blank)	2. REPORT DATE 25 May 01	3. REPORT TYPE AND DATES COVERED Final Report, 1 June 00 - 1 Feb 01

4. TITLE AND SUBTITLE

MEMS RF Switches with Ultra-High Switching Speeds

5. FUNDING NUMBERS

C DAAH01-00-C-R146

6. AUTHOR(S)

Frank T. Djuth[1], Qingqi Zhang[1], Susan Trolier-McKinstry[2],
Srinivas Tadigadapa[2], Thomas N. Jackson[2], Steven J. Gross[2]

7. PERFORMING ORGANIZATION NAME(S) AND ADDRESS(ES)

[1] Geospace Research, Inc.
550 N. Continental Boulevard, Suite 110, El Segundo, CA 90245
[2] The Pennsylvania State University
University Park, PA 16802

8. PERFORMING ORGANIZATION REPORT NUMBER

GRI-SB-01-7510

9. SPONSORING / MONITORING AGENCY NAME(S) AND ADDRESS(ES)

U.S. Army Aviation and Missile Command
Weapons Sciences Directorate, AMRDEC
Redstone Arsenal, AL 35898-5000

10. SPONSORING / MONITORING AGENCY REPORT NUMBER

11. SUPPLEMENTARY NOTES

The views and conclusions contained in this document are those of the authors and should not be interpreted as representing the official policies, either express or implied, of the Defense Advanced Research Projects Agency or the U. S. Government.

12a. DISTRIBUTION / AVAILABILITY STATEMENT

Approved for public release; distribution unlimited.

12b. DISTRIBUTION CODE

13. ABSTRACT (Maximum 200 words)

The objective of this program was to validate a new actuator for high-speed, radio-frequency (RF) switches and to develop methodologies for its fabrication. Special attention is placed on switch performance at frequencies between 12-18 GHz. The switch is predicated on thin-film microelectromechanical systems (MEMS) technology with piezoelectric actuation. In general, piezoelectric materials develop strain when an electric field is present, which allows mechanical expansion and contraction of the material to be controlled by an applied voltage. Unlike traditional electrostatic MEMS switches, the closing force between the metal-to-metal contacts can be significantly improved by increasing the bias voltage (electric field strength) across the piezoelectric material. Because the switch restoring force is large, in-use stiction is greatly mitigated with this architecture. The piezoelectric material lead zirconate titanate (PZT) proved to be a viable actuator for high-speed switches. Three strategies are suggested for lowering the switch time constant into the tens of nanoseconds range while preserving other important characteristics of the switch (e.g. high isolation, low resistive losses). These include a bimorph design, piezoelectric extensional bars, and flextensional actuators. Combinations of these strategies are likely to yield a high-performance switch.

14. SUBJECT TERMS

Microelectromechanical Systems, MEMS, RF Switch, Microwaves, Lead Zirconate Titanate, Thin Film, PZT

15. NUMBER OF PAGES
54

16. PRICE CODE

17. SECURITY CLASSIFICATION OF REPORT	18. SECURITY CLASSIFICATION OF THIS PAGE	19. SECURITY CLASSIFICATION OF ABSTRACT	20. LIMITATION OF ABSTRACT
Unclassified	Unclassified	Unclassified	UL

TABLE OF CONTENTS

1. Introduction

The RF switch designed in Phase 1 is predicated on thin-film MEMS technology with piezoelectric actuation. In general, piezoelectric materials develop strain when an electric field is present, which allows mechanical expansion and contraction of the material to be controlled by an applied voltage. The piezoelectric material lead zirconate titanate (PZT) is employed in the current program. The formula for the PZT thin film compound is usually expressed as $PbZr_{0.6}Ti_{0.4}O_3$, where the "x" in $PbZr_{1-x}Ti_xO_3$ denotes relative composition. Compositions near the morphotropic phase boundary (i.e. the boundary between rhombohedral and tetragonal phases at $PbZr_{0.53}Ti_{0.47}O_3$) have the largest piezoelectric constants. The overall actuation technique and fabrication process were validated as part of the Phase 1 research program. Unlike traditional electrostatic MEMS switches, the closing force between the metal-to-metal contacts and the switching speed can be significantly improved by increasing the bias voltage (electric field strength) across the piezoelectric material. The PZT-based actuator also mitigates stiction after release (i.e., in-use stiction) because of its greater than normal restoring force. In-use stiction remains a fundamental reliability issue in traditional MEMS switches that are actuated electrostatically.

The principal objective of the Phase 1 effort was to validate a sol-gel PZT actuator for use in MEMS RF switches and in so doing determine the feasibility of using this actuator for high-speed switching. This entails the development of fabrication and production techniques for the PZT switch, which represents a significant part of the effort.

The RF MEMs switch utilizes piezoelectric actuation as an alternative to mitigate many of the unwanted features of electrostatic actuation such as slow speed, high operating voltage, and stiction. Piezoelectric materials such as lead zirconate titanate (PZT) develop a strain when an electric field is applied, so that mechanical expansion and contraction of the material can be controlled with an applied voltage [1, 2]. In the unimorph cantilever design under examination, the piezoelectric material is deposited on top of a thin layer of Si_3N_4 that provides mechanical stiffness. Here, the piezoelectric layer serves as the driving element while the Si_3N_4 layer serves as the passive element against which a bending moment is developed. The closing force of the switch is determined by the dimensions and mechanical rigidity of the cantilever along with the strain in the piezoelectric layer, where the strain of the piezoelectric material, S_i, is equal to the piezoelectric constant, d_{ki}, multiplied by the electric field strength, E_k. Unlike traditional electrostatic MEMS switches, the closing force between the metal-to-metal contacts can be significantly improved by increasing the bias voltage (electric field strength) across the piezoelectric material.

The Phase 1 research made use of a standard cantilever design. The cantilever is unimorph in nature and utilizes a single layer of PZT. Two approaches were investigated: one in which activation was achieved with piezoelectric strain transverse to the imposed electric field (d_{31}) and one in which the strain was parallel to the imposed field (d_{33}). A cantilever design was employed in Phase 1 because its mechanical properties were well-understood [3]. This eliminated the need for an extensive mechanical study and allowed us to concentrate on more pressing issues central to the success of Phase 2. The low resonance frequency of the cantilever limits the switching times of the Phase 1 prototype to the low μs regime. Nevertheless, Phase 1 served as a test bed for fabrication techniques to be employed during Phase 2.

The validation of PZT actuators in Phase 1 makes new mechanical designs feasible in the future that will lower the switch time constant into the tens of nanoseconds range (e.g., multi-layer PZT stacks with linear (d_{31}) piezoelectric strain modes). The actuation time of PZT is ~100 ps, so in itself it does not pose a constraint on the desired switching times. Mechanical design determines the switch speed. The use of higher electrode voltages allows the MEMS switch to be smaller and stiffer, giving rise to much shorter time constants.

For fast switches, linear actuators designed for operation in the d_{31} mode are required if low voltage operation is desirable. However, if higher voltages can be tolerated, the d_{33} mode has specific advantages. Because the d_{33} mode has slightly more than twice the strain of d_{31} for the same dimensions and operating field, shorter (stiffer) actuators can be used for a given switch travel which results in a higher resonant frequency and faster switch operation. This can be accomplished by surface electrodes, but stacked d_{31} electrode designs are also of interest. One approach is to fabricate multi-layer stacked actuators using low-cost ceramic tape casting similar to that used for ceramic capacitor manufacturing. To allow low-voltage operation, thin layers (<2 μm) would be used, and a typical switch actuator would have tens or even hundreds of layers.

Although linear switch actuators provide a relatively simple path to high speed switches, the approach of using a small, stiff, and relatively low mass actuator to obtain a high resonant frequency is quite general, and alternative designs are possible. Composite flextensional actuators (so-called moonies, rainbows, cymbals, and similar devices) are of particular interest since they can provide relatively large displacement (for good switch isolation) with relatively large stiffness and generative forces compared to simple bending actuators. Well-designed composite flextensional actuators can have an effective d_{31} or d_{33} many times larger than the piezoelectric material alone and thus are intriguing candidates for miniaturization and integration as high-speed MEMS RF switches.

2. Summary of the Phase 1 Study

During Phase 1, a fully functioning cantilever operating in the d_{31} actuation mode was successfully tested. Final tests of the d_{33} mode were delayed because of the availability of materials, in particular, Si wafers layered with LTO (SiO_2) and Si_3N_4. Most of the 18 four-inch wafers used during Phase 1 were dedicated to d_{31} studies. The d_{33} tests were subsequently performed after the Phase 1 period.

As noted above, piezoelectric materials such as lead zirconate titanate (PZT) develop a strain when an electric field is applied, so that mechanical expansion and contraction of the material can be controlled with an applied voltage [1, 2]. In the unimorph cantilever design that was implemented in Phase 1, the piezoelectric material is deposited on top of a thin layer of Si_3N_4 that provides mechanical stiffness. Here, the piezoelectric layer serves as the driving element while the Si_3N_4 layer serves as the passive element against which a bending moment is developed. The closing force of the switch is determined by the dimensions and mechanical rigidity of the cantilever along with the strain in the piezoelectric layer, where the strain of the piezoelectric material, S_i, is equal to the piezoelectric constant, d_{ki}, multiplied by the electric field strength, E_k. Unlike traditional electrostatic MEMS switches, the closing force between the metal-to-metal contacts can be significantly improved by increasing the bias voltage (electric field strength) across the piezoelectric material.

A cantilever design was employed in Phase 1 because its mechanical properties were well-understood [3]. This eliminated the need for an extensive mechanical study and allowed us to concentrate on more pressing issues central to the success of Phase 2. The low resonance frequency of the cantilever limits the switching times of the Phase 1 prototype to the low μs regime. Nevertheless, Phase 1 served as a test bed for fabrication techniques to be employed during Phase 2.

In Phase 1 we verified that a PZT thin film is a viable actuator for RF switches operating in both the d_{31} mode (bias voltage across the thickness of the cantilever) and the d_{33} mode (bias voltage interdigitated parallel to the cantilever beam). These two modes of actuation are illustrated in Figures 1 and 2. Verification of the MEMS actuator was accomplished through laboratory tests aimed at applying PZT to stacked substrate layers to be used in the fabrication of switches. Subsequent tests on the PZT thin film indicated that its piezoelectric properties were intact and ideally suited for its role as an actuator. In addition, for d_{33} operation the required passivating layer (ZrO_2) between the PZT film and the silicon-based substrates was successfully tested.

A variety of critical tests for d_{31} and d_{33} operation were successfully conducted during Phase 1. These included verification that a cantilever step generated by the signal line in the unimorph design will not impact the annealing of PZT to the cantilever. Additionally, we have been able to optimize the design of the interdigitated electrodes used for d_{33} operations. In this regard, an enlarged electrode test fixture was designed so that enough current could be measured to determine the homogeneity of the electrode electric field in the PZT thin film. Other items such as the cantilever release process, the etching of the component layers of the switch, and strategies for protecting the PZT from the HF used for the sacrificial etch have been resolved. As in any research program of this nature, some of the fabrication techniques thought to be viable turned out to be problematic. For example, wet etching of the ZrO_2 layer along with the PZT layer proved not to be feasible because of the hardness of the ZrO_2. Instead, ion milling had to be adopted. Moreover, the ion milling etching of the cantilever itself had to be adjusted because of cracking of the positive photoresist material.

In Phase 1, a successful fabrication and release methodology for cantilever switches was implemented. The proper range of cantilever motion for d_{31} operations was established and the cantilever time constants were consistent with theoretical expectations. Limited tests were also performed with the d_{33} cantilever configuration. At comparable driving voltages, the d_{33} displacement is about half that of d_{31}. The reason for this is the dead space created on the PZT by the surface electrodes and the generally lower electric field strengths that are produced by interdigitated electrodes. Unless high electrode voltages are available, d_{31} is the preferred mode of operation for PZT-actuated switches.
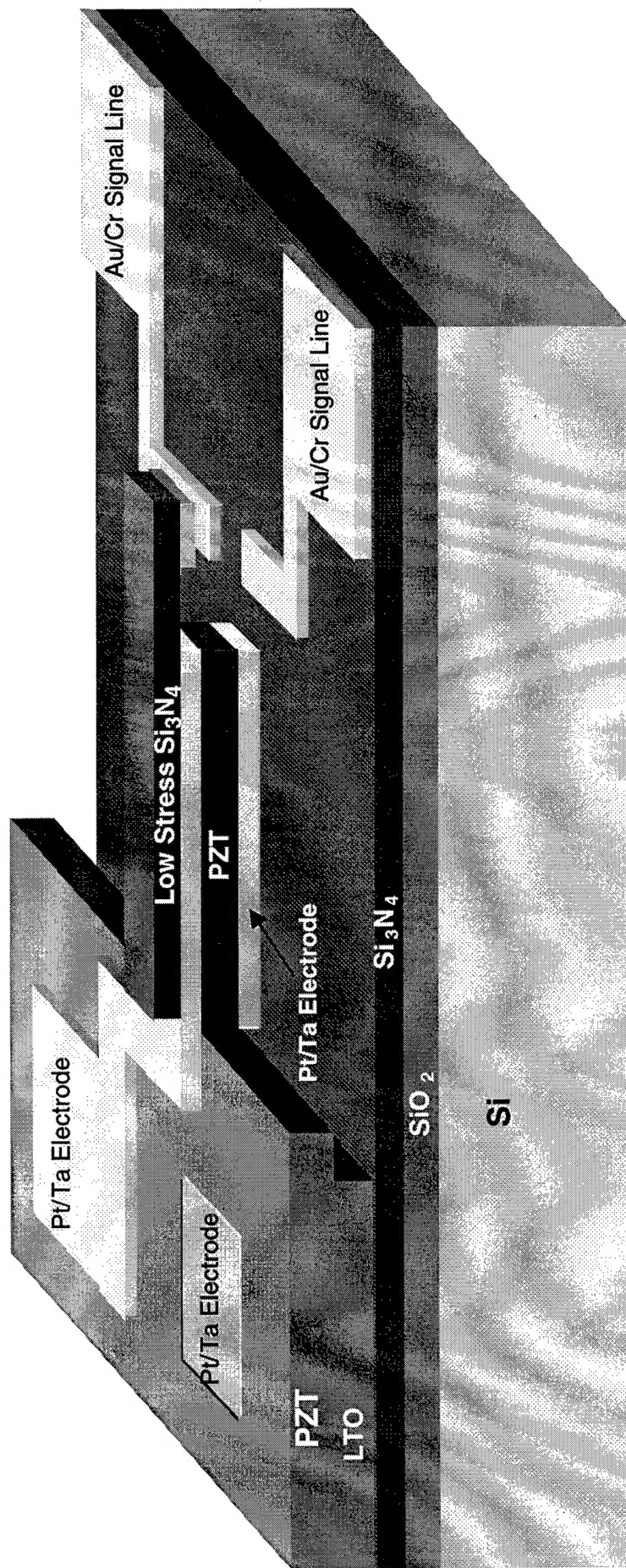
Figure 1. Schematic illustration of a d_{31}-actuated cantilever switch. Alternatively, the Si/SiO2/Si3N4 substrate can be replaced with either a low-k ceramic (LTCC) or a GaAs substrate to reduce signal losses.
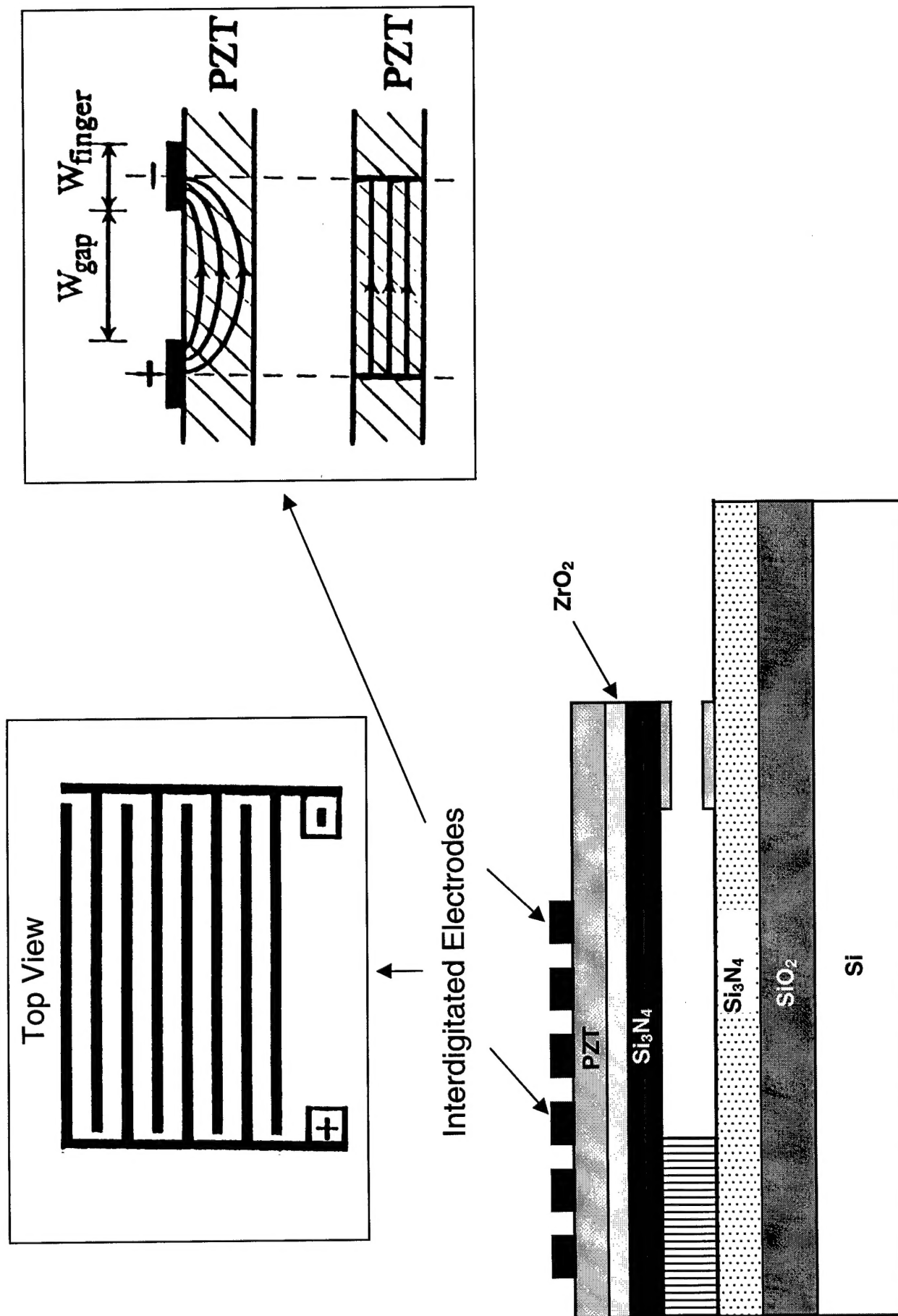
4

Figure 2. Illustration of a D$_{33}$ Cantilever design

5

3. Characterization of the PZT Actuator

Although many laboratory tests were performed during Phase 1, we outline only the most important results here. Because sol-gel PZT had been previously used only with bulk ceramics, it was important to establish that the process used for preparation of the PZT thin-film can be readily implemented and that the ferroelectric properties of the thin film are preserved during the MEMS fabrication process. Complex and/or delicate fabrication techniques are not conducive to the manufacturing process.

The sol-gel thin-film process proved to be rather robust and can easily be implemented in the manufacturing environment of a foundry. However, the foundry must be capable of handling the lead contaminants produced as part of the heating of the PZT. Several foundries have been identified that will accept PZT processing. The production procedure is outlined in Figure 3 below. Approximately one day is required to form the precursor solution (Figure 3a). The sol-gel process is completed in about an hour on the following day. This principally entails ~ 1-min spinning at 100 C, 1 min on a "hot plate" at 300-400 C, and the firing of the RTA (furnace) for about 5 min per pass (see Figure 3b).

3.1 d_{31} Mode of Operation

With the aid of X-ray diffraction techniques it was established that the final PZT thin films had a crystalline structure consistent with the preferred perovskite phase [4-7]. PZT was prepared on a Pt (111) substrate to test the PZT-electrode interface for d_{31} switch activation. The bottom portion of the substrate contained SiO_2 and Si. (See Figure 4.) The surface microstructure is often revealed with the aid of X-Ray Diffraction (XRD), using the small angle diffraction method. XRD patterns in all thin films ≤ 5μm tend to show measurable (111) preferred orientation in the plane of the substrate. For the measurement shown in Figure 4, the "normal" theta-2theta method was employed in which X-ray intensity was contributed from the entire sample. Consequently the Pt (111) peak is also observed in the pattern. The PZT has a pure perovskite phase [3] and a strong (111) orientation. This is expected in a properly formed PZT-Pt interface. The strong PZT (111) peak is consistent with PZT crystallization proceeding preferentially by heterogeneous nucleation and growth from the bottom heteroexpitaxial (111) Pt electrode. This occurs because of close lattice matching between PZT and Pt.

In optimized solution-deposited PZT films, the dielectric and ferroelectric properties typically are comparable to those of bulk ceramics. A case in point is the well-formed hysteresis loop shown in Figure 5 for the case of PZT on Pt (111) substrate. The polarizing of the PZT (so-called poling) was performed at room temperature. The PZT film possessed the expected polarization electric field hysteresis loop. The remnant polarization was $P_r=25$ $\mu C/cm^2$, and the coercive field was $E_c=46$ kV/cm. This is typical of a well-formed PZT thin film.

Figure 6a illustrates how d_{31} increases with increasing polarizing (poling) field strength. The saturation of d_{31} occurs near 40 pC/N at a poling field of about three times the coercive field strength (or approximately 30 V in the figure). In Figure 6b, a gradual decrease in d_{31} with time (aging) is observed to occur over time scales of several hours. However, this aging process can be mitigated by poling at an elevated temperature (~120 C). Alternatively, one can achieve a similar effect by poling while exposing the sample to ultraviolet radiation. The precise reduction in the aging effect depends in large part on the processing of the film. Nevertheless a substantial improvement can be anticipated. In general, the aging reduction process is implemented once the production process is finalized as part of an optimization procedure.
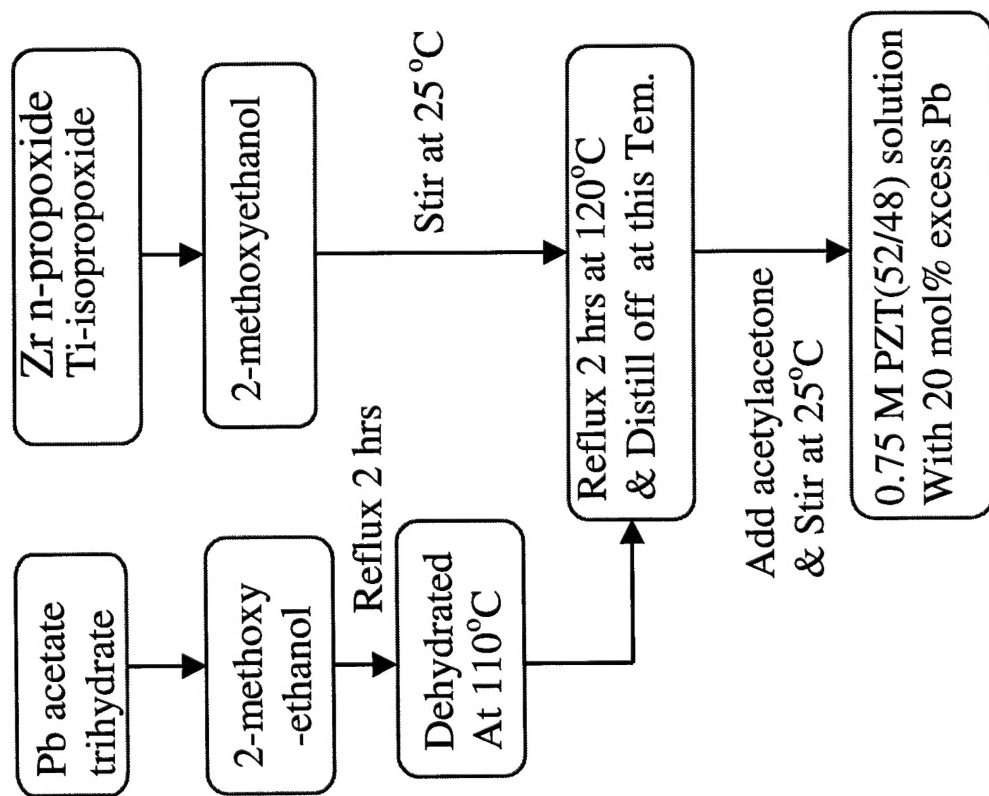
6

Figure 3b. Final processing of the PZT thin film.

Figure 3a. Flow diagram illustrating the preparation of PZT thin film precursor solution.
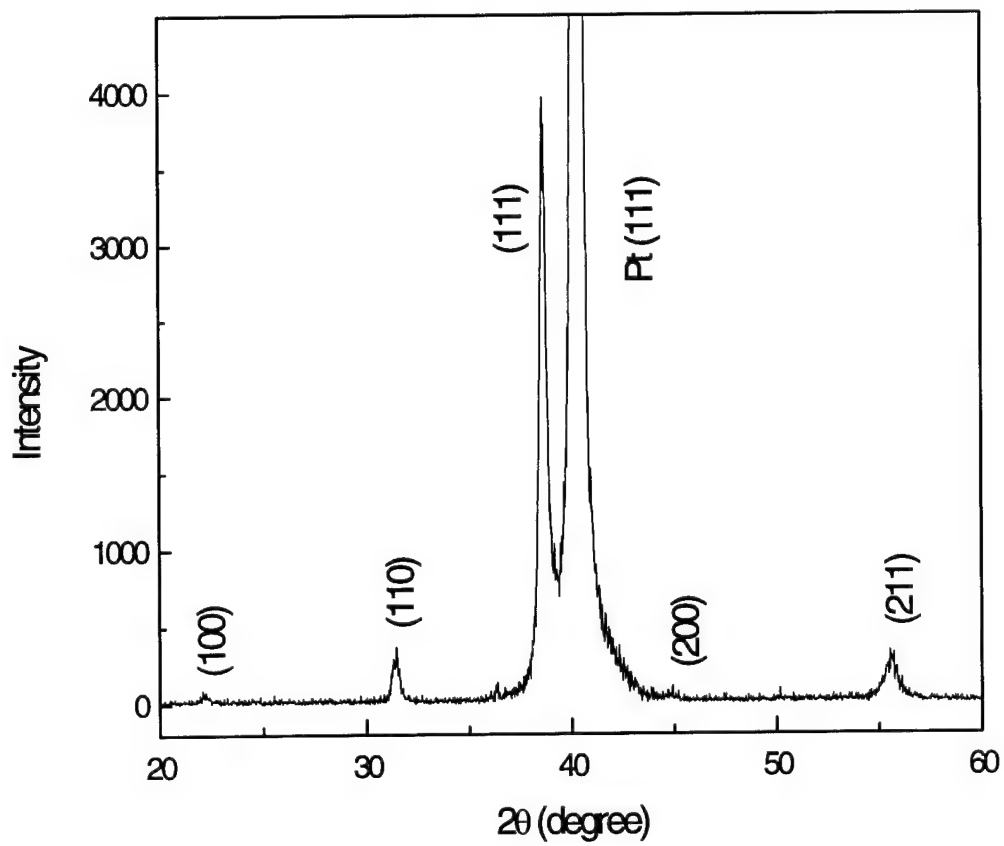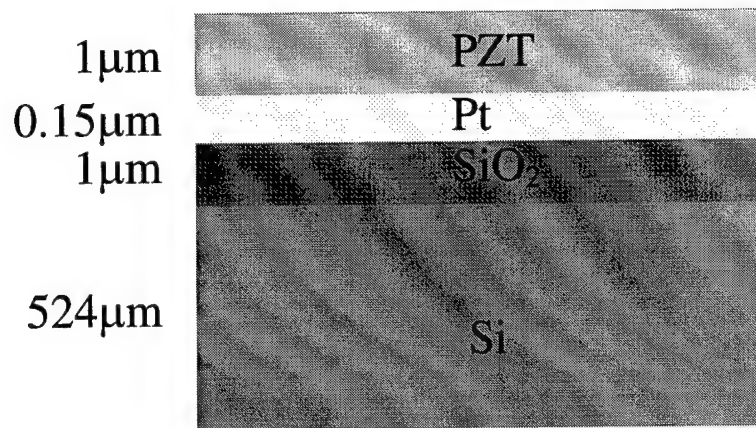
7
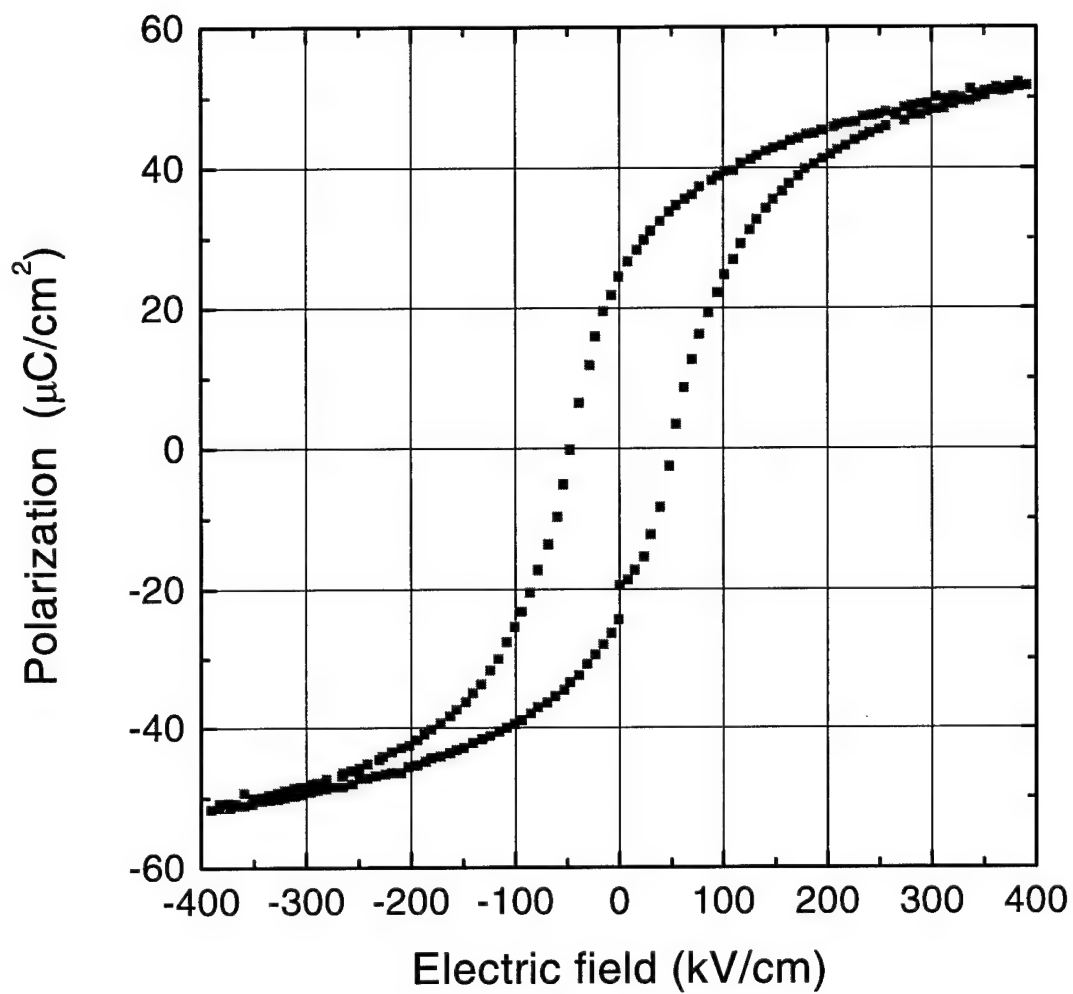
Figure 4. Preparation of PZT film on Pt-(111) substrate.

Figure 5. Polarization-Electric Field Hysteresis Loop measured with a RT66A ferroelectric tester. The remnant polarization and coercive field were 25 C/cm² and 46kV/cm, respectively.
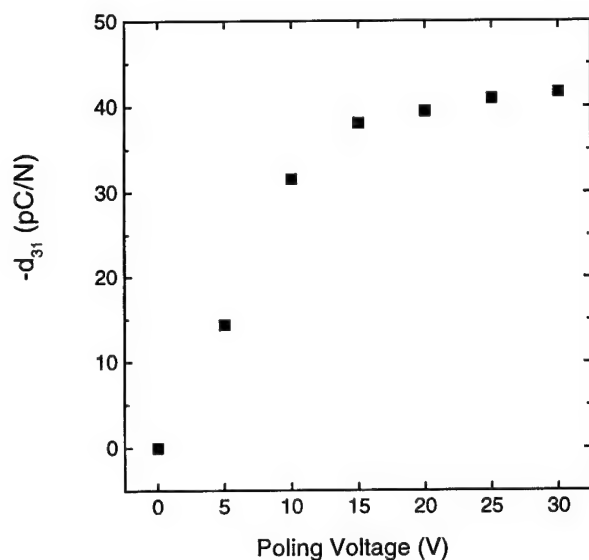
Figure 6a. d_{31} increased with increasing poling field/voltage and reached a saturation value of about 40 pC/N at $3E_c$.
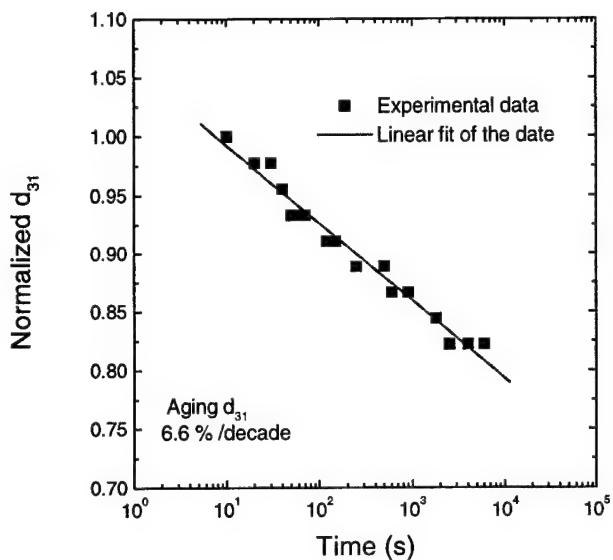
Figure 6b. d_{31} gradually decreased with time after poling at a rate of about 6.6% per decade.
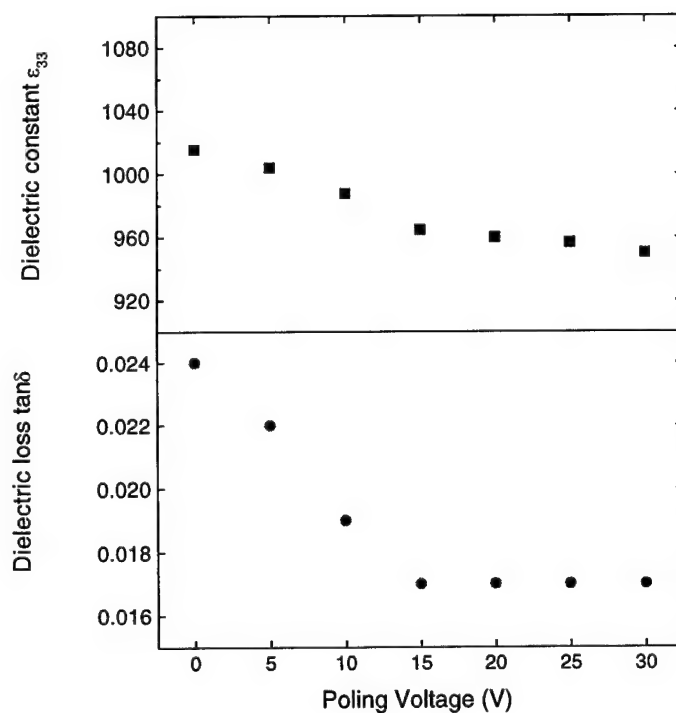
Figure 7. Dielectric constant and loss tan of the PZT film measured at a frequency of 1 kHz.

The dielectric characteristics of the PZT film are illustrated in Figure 7 above. The dielectric constant ε_{33} and the loss tanδ were measured at a frequency of 1 kHz using a 4192 LF impedance analyzer. As the poling voltage increases, ε_{33} and the loss tanδ reaching values near ε_{33} ~950 and tanδ ~1.7% for poling electric fields near three times E_c. These are general features of ferroelectric material. The dielectric constant and loss tangent in the poling direction decrease after poling because the polarization has switched to the direction of the poling field. The reduction in the dielectric loss with increasing poling voltage is a beneficial feature.

3.2 d_{33} Mode of Operation

The assembly strategy for d_{33} switch operation has one distinctive difference in comparison with d_{31}. In the fabrication of a d_{31} switch Pt or Pt/Ti serves to isolate the PZT from SiO_2. For d_{33} actuation, interdigitated electrodes are used, and as a result, a barrier with low dielectric constant has to be constructed between the PZT and Si_3N_4/SiO_2. Our strategy in this case is to use ZrO_2 to passivate the silicon substrates. ZrO_2 is a thin film that is applied by the sol-gel process similar to PZT. In past tests where PZT, ZrO_2, SiO_2, and Si have been stacked together, strong symmetric dielectric hysteresis was observed from the transverse field generated via interdigitated surface electrodes [Y. Xu, private communication, 2001]. This indicates that the PZT is exhibiting excellent ferroelectric properties and very good transverse coherence.

In order to determine the viability of using ZrO_2 to passivate silicon substrates, PZT film was placed on a substrate of $ZrO_2/SiO_2/Si$ and XRD patterns were measured. This is illustrated in Figure 8 below. The perovskite phase was observed in the PZT thin film, and the structure of the PZT film was random without orientation. It can be seen from the bottom trace of the XRD plot that the ZrO_2 layer is mainly amorphous after annealing because of the high refractory nature of ZrO_2. However, the PZT film (top trace) has a well-formed perovskite structure phase. The peak with highest intensity in the PZT XRD plot is indexed as 110, indicating that the film is mostly randomly oriented. This is not surprising because the PZT film was grown on an amorphous surface. (In actuality, PZT is rhombohedral, and the (110) and (101) peaks overlap. One could label the peak (101,110), but this does not alter the above conclusion.)

The same type of substrate combination ($ZrO_2/SiO_2/Si$) was also used to determine the feasibility of putting Au/Cr interdigitated electrodes on the surface of PZT. The methodology used in these tests is illustrated in Figure 9. The key sub-process in this regard is the Buffered Oxide Etch (BOE). Overall, the procedure outlined in Figure 9 appears to provide an effective means for the laydown of interdigitated electrodes.

PZT was also placed on the substrate combination $ZrO_2/Si_3N_4/SiO_2/Si$. This is a layer combination that we currently plan on using in the MEMS RF switch design (discussed below). Figure 10 shows the XRD results, which are as expected. However, some cracking was observed in the ZrO_2 layer. This was subsequently mitigated by improving the sol-gel process for ZrO_2 Adjustments in solution concentration, spinning speed, and annealing temperature were made.

Finally, many PZT thin films were prepared on $ZrO_2/Si_3N_4/SiO_2/Si$ with an anchor formed by partially etching away the SiO_2 substrate. The objective was to verify that there would be no cracking of the ceramics on flat surfaces or the corner surfaces for various sizes of anchors. This test was completely successful in that no cracks were detected. In Figure 11, optical micrographs are used to illustrate the results. At left with low magnification, cracks are

1μm   PZT

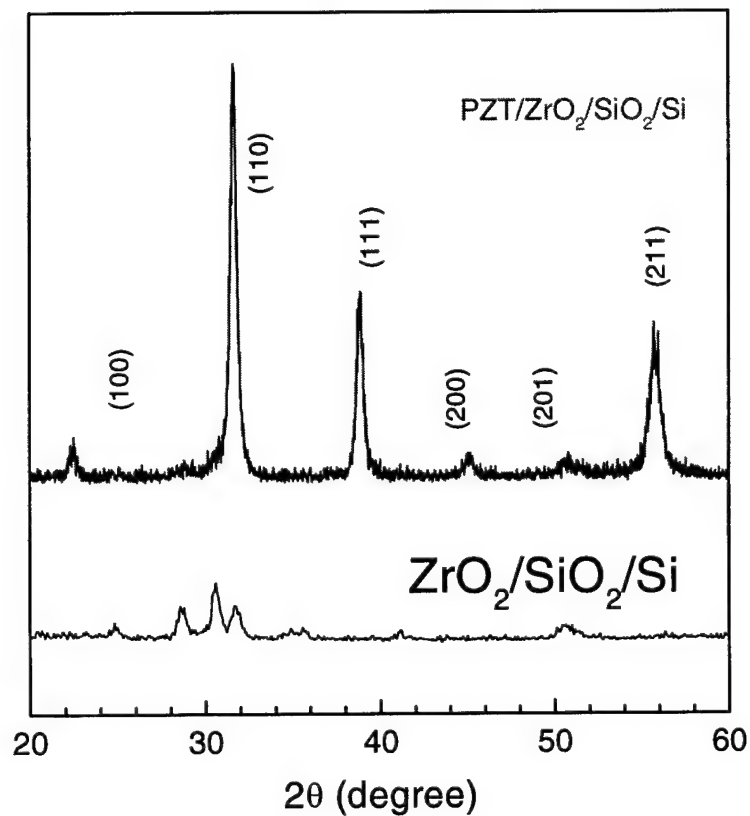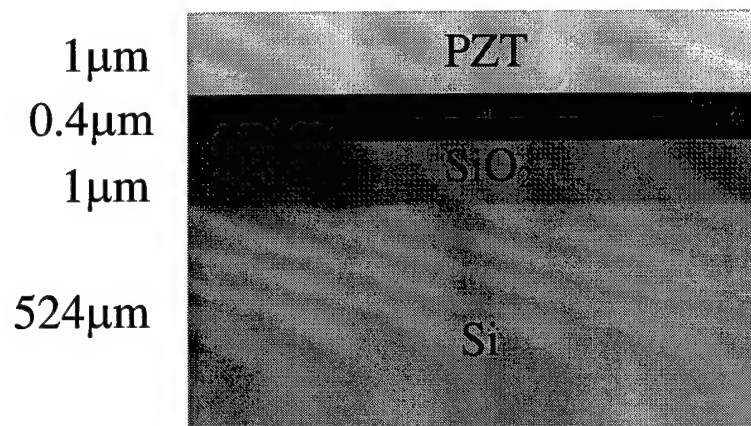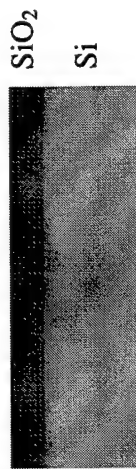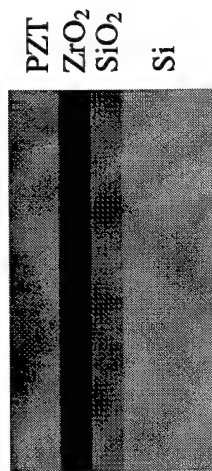0.4μm

1μm   SiO₂

524μm   Si

Figure 8. Pure perovskite phase was observed in the PZT film, and the structure was random without orientation.

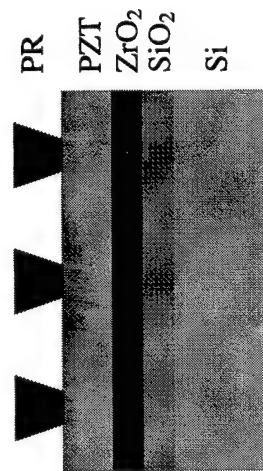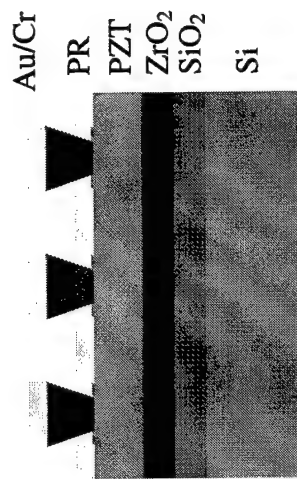1.Start: SiO$_2$/Si

2.spin coating ZrO$_2$ and PZT and etch the edge using BOE

3.Lithography (using BPRS 100 as photoresist) and oxygen plasma for residue PR
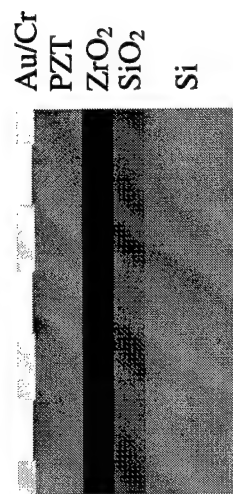
4.Evaporator Au/Cr

5.Liftoff

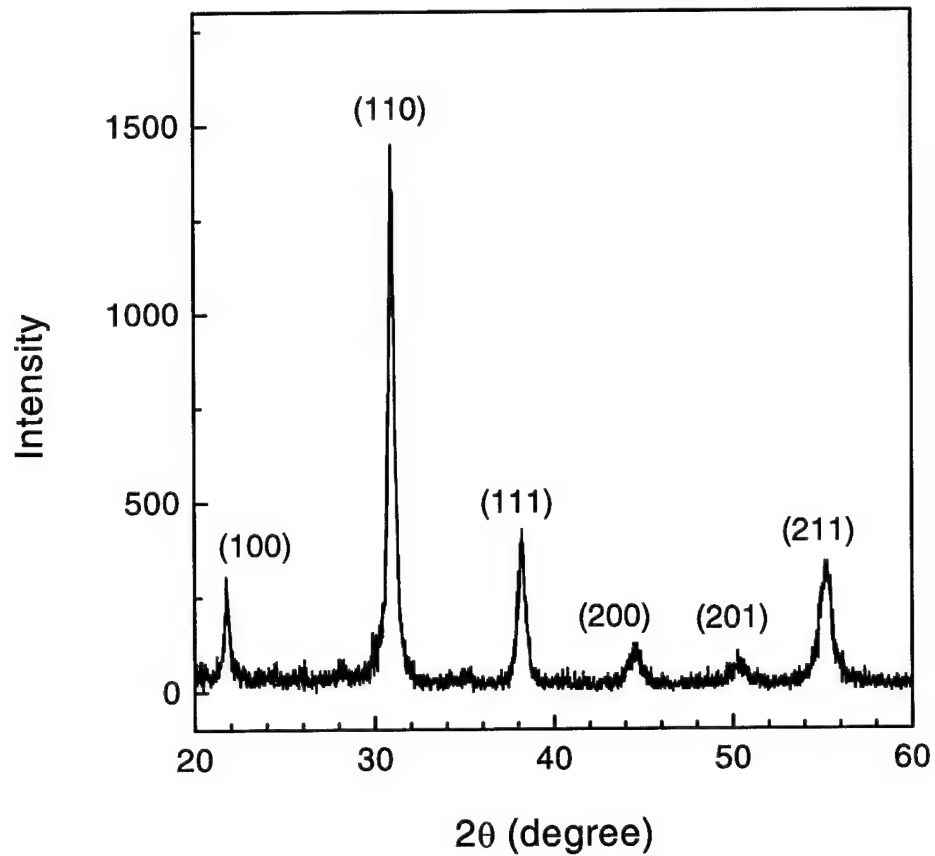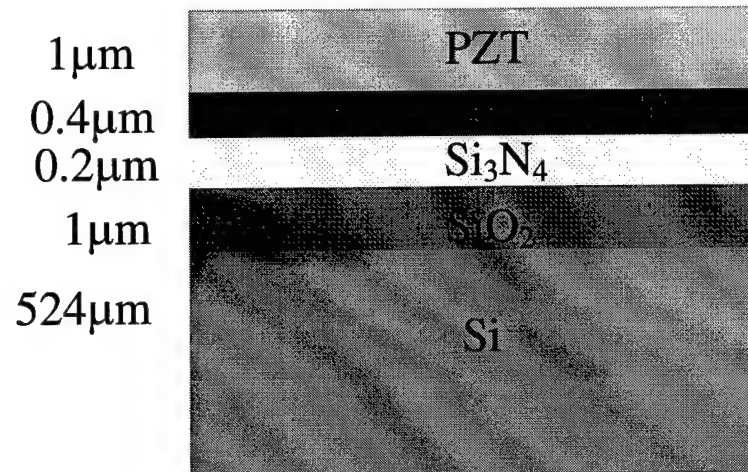Figure 9. Schematic illustration of the process used to place Au/Cr interdigitated electrodes on the surface of PZT

13

Figure 10. Preparation of a PZT thin film on a ZrO2/Si3/SiO2/Si substrate.
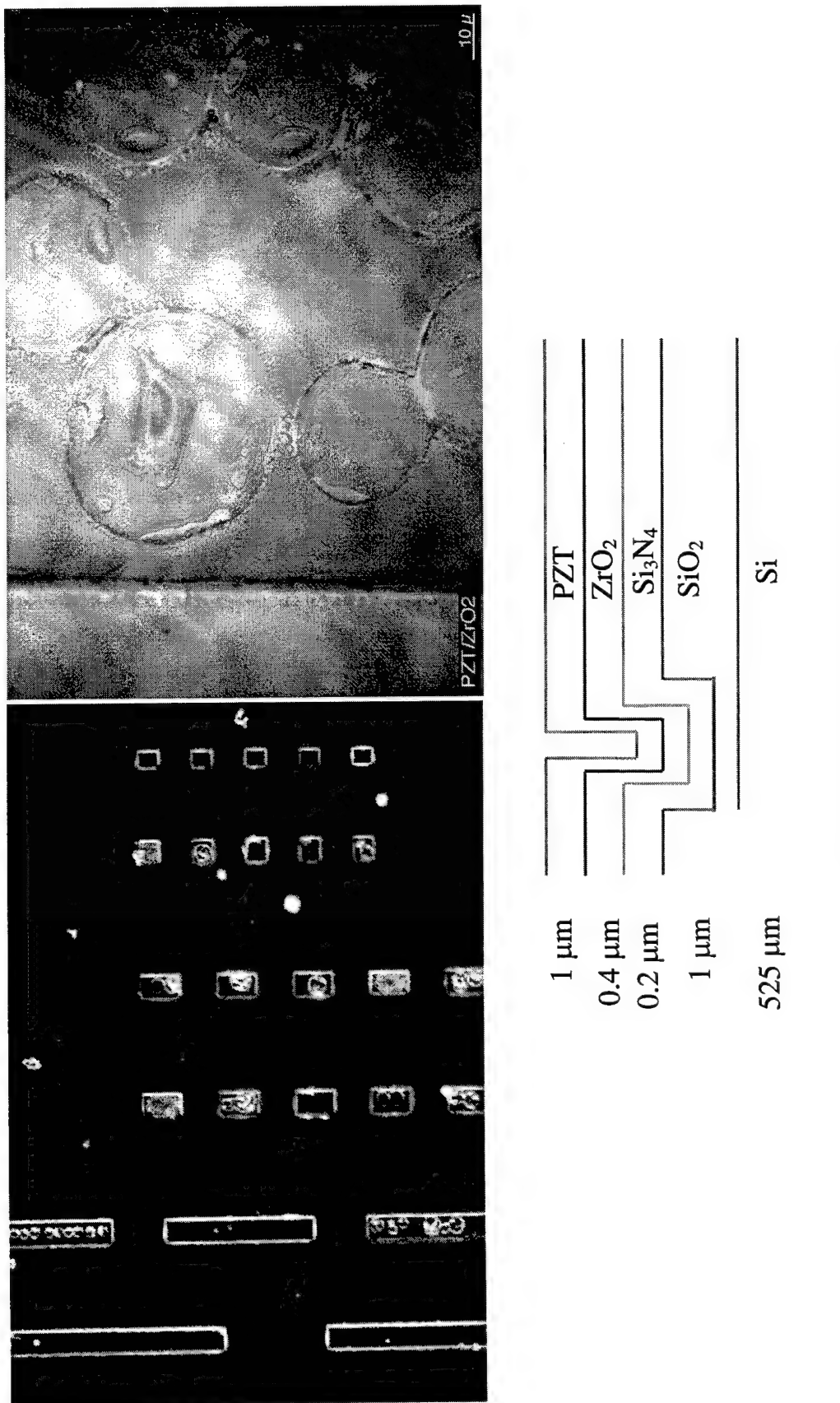
Figure 11. Samples of PZT film on $ZrO_2/Si_3N_4/SiO_2/Si$ with anchors formed by etching away part of the SiO_2.

15

not evident in the flat surfaces. On the right, with high magnification, the edge of the anchor is also observed not to crack. (PZT grain structure can also be seen in this figure.)

It is noteworthy that the above test is a precursor to the freeing of cantilevers, the next major step in the MEMS process. By etching away the SiO_2 in Figure 11, we are left with the d_{33} cantilever.

In optimized solution-deposited PZT films, the dielectric and ferroelectric properties typically are comparable to those of bulk ceramics. A case in point is the well formed hysteresis loops shown for the case of PZT on Pt (111) substrate in Figure 12a. For the d_{33} study, we employed interdigitated electrodes having ten fingers. The polarizing of the PZT (so-called poling) was performed at room temperature. The PZT film possessed the expected polarization electric field hysteresis loop. The remnant polarization was P_r=39 $\mu C/cm^2$, and the coercive field was E_c=48 kV/cm. This is typical of a good PZT thin film.

Figure 12b illustrates how P_r and E_c increase with increasing polarizing (poling) field strength. In this case the thickness of the PZT layer was 1 μm. The saturation of these two values occurs at a poling field of about five times the coercive field strength. At saturation, the dielectric constant and loss tangent are 1112 and .013, respectively. The capacitance is 3.2 pF. In Figure 12c, d_{33} is shown as a function of poling voltage. The poling was performed at room temperature. At saturation, the value of d_{33} is 103 pC/N, which is more than twice that typically encountered for d_{31}. This agrees with theoretical expectations. The resulting strain for d_{33} is about twice that of d_{31}, making d_{33} the preferred mode for switch design.

3.2.1 Etching ZrO_2 for D_{33} Switch Operations

In the prototype stage, the etching technique used to define the cantilever was dictated by expediency. Within this context, it is generally easier to wet etch a substrate than to dry etch one. A key issue centered on how to etch ZrO_2, which is a fairly hard material. Any etching formula that could successfully be used with ZrO_2 could in principle also be used to etch the PZT layer. A wet etch formula developed by Dr. Adair at Draper Laboratories was optimistically assumed to be an effective etching agent. The so-called Draper formula is presented below.

> 4.375 g EDTA Disodium
> 11g NH_4Cl
> 200 ml H_2O
> 15.5 ml acetic acid
> 15.5 ml nitric acid (70% HNO_3)
> 15.5 ml hydrochloric acid (37% HCl)
> 2 ml BOE (Buffered Oxide Etch 10:1)

Unfortunately this formula was not effective as a ZrO_2 etchant even when it was warmed up to 70 C. This is illustrated in Figure 13, which shows that the Draper formula is not effective in etching ZrO_2. As expected, it was effective on PZT. A search was subsequently launched to find a wet etchant that would successfully work with both ZrO_2 and PZT. Twelve formulae shown in Table 1 were tested on ZrO_2. One formula was found to be an effective etchant (HNO_3:BOE:H_2O). However, because HNO_3:BOE:H_2O severely undercuts PZT, one must use a two step process. First the Draper formula is used to etch PZT. PZT is then masked and HNO_3:BOE:H_2O is applied. The HNO_3:BOE:H_2O formula was not used because it was difficult to control. Initially we used the Draper formula to etch PZT, and then dry etched ZrO_2 using an ion milling technique. Figure 14 provides an example where PZT is wet etched with the
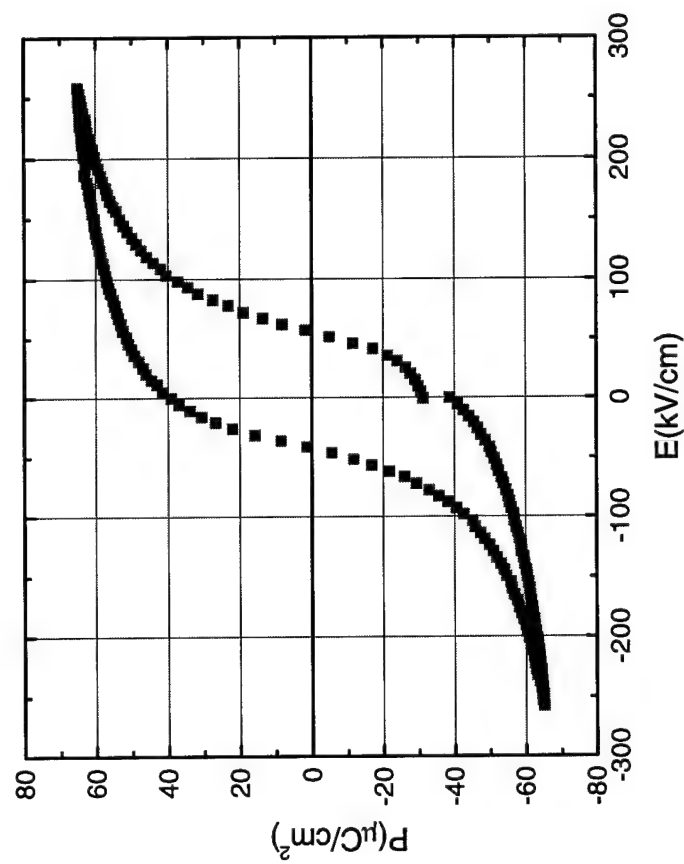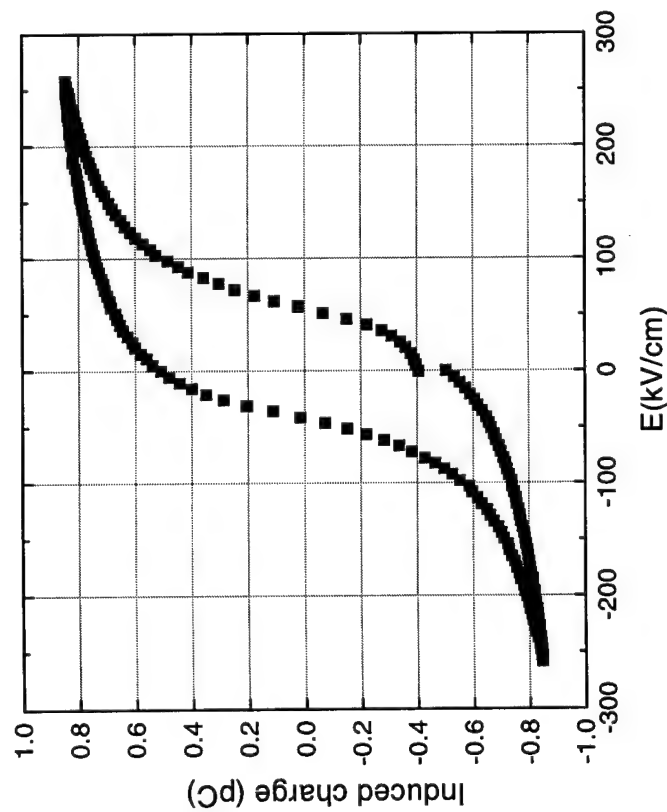
Figure 12a. Induced Charge-Electric Field and Polarization-Electric Field hysteresis loops for a PZT thin film with an interdigitated electrode. The interdigitated electrode had 10 fingers each 100 microns in length. The finger width and finger gap were both 4 microns. The measured remnant polarization and coercive field were 39 $\mu C/cm^2$ and 48 kV/cm, respectively.

17

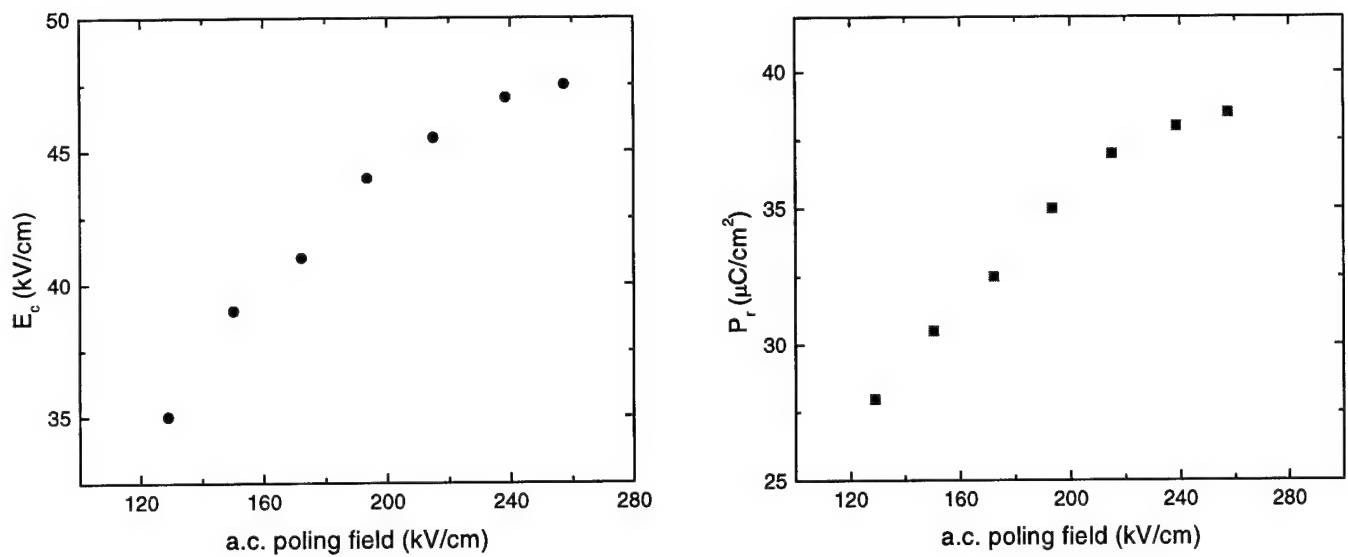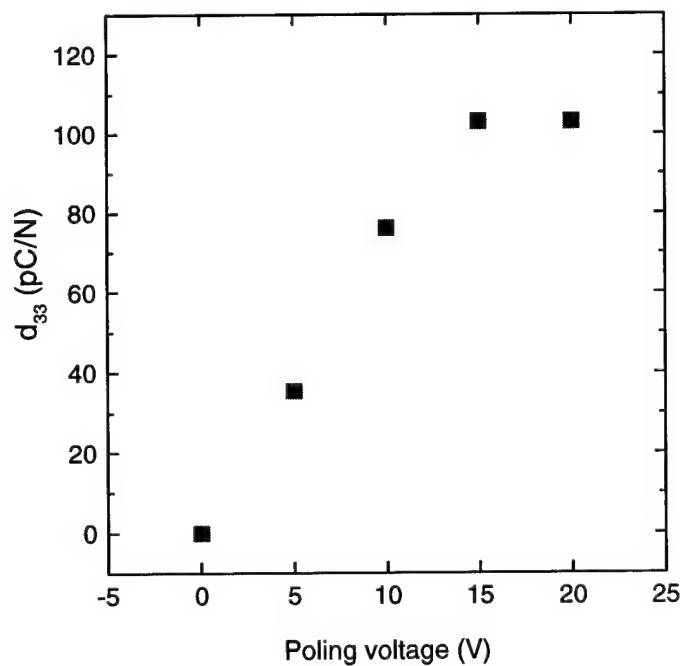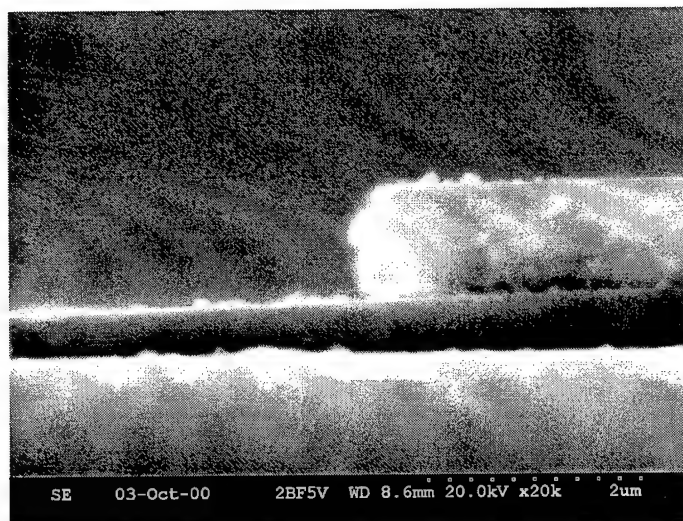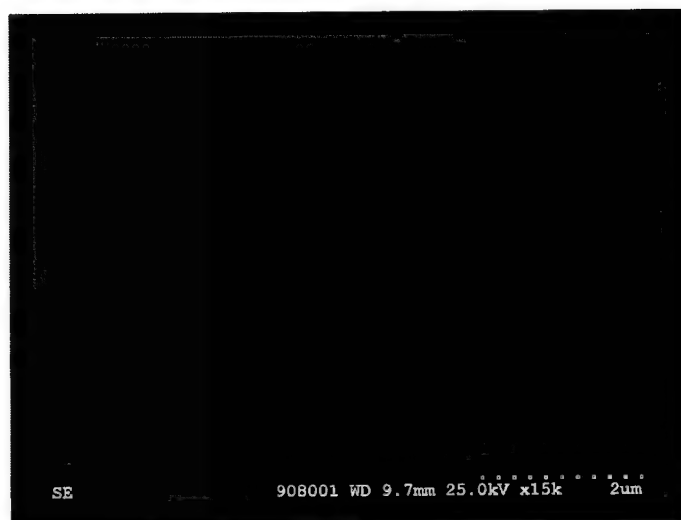Figure 12b. Dependence of the remnant polarization P_r and the coercive field E_c on a.c. poling field.

Figure 12c. d_{33} increases with increasing poling field and reaches a saturation value of 103 pC/N at a poling field of about $3E_c$.

Etching time 10 mins

Etching time 22 mins

Figure 13. Etching of a PZT thin film on a ZrO_2/Si_3N_4 substrate. The results show that ZrO_2 cannot be etched with the Draper formula.

Table 1. Solutions tested for the etching of ZrO_2

Solution	Temperature (^{o}C)	Result
HF	Room Temperature	Etches PZT into small pieces
HCl:BOE:H$_2$O	Room Temperature	Etches PZT into small pieces
10 ml HNO$_3$ 1.2 ml BOE 10 ml H$_2$O	Room Temperature Must agitate in an ultrasonic bath for 1 min	Severely undercuts PZT but also etches ZrO_2 well
HNO$_3$:HF:H$_2$O	Room Temperature	Etches PZT into small pieces
HCl	Room Temperature, 70-80°C	Does not etch ZrO_2
H$_2$SO$_4$	Room Temperature, 70-80°C	Does not etch ZrO_2
HNO$_3$	Room Temperature, 70°C	Does not etch ZrO_2
H$_2$C$_2$O$_4$	Room Temperature, 70-80°C	Does not etch ZrO_2
HAc	Room Temperature, 70°C	Does not etch ZrO_2
NaOH	70-80°C	Does not etch ZrO_2
NH$_4$OH	Room Temperature, 70°C	Does not etch ZrO_2
H$_2$O$_2$:HCl:H$_2$O	Room Temperature, 70°C	Does not etch ZrO_2
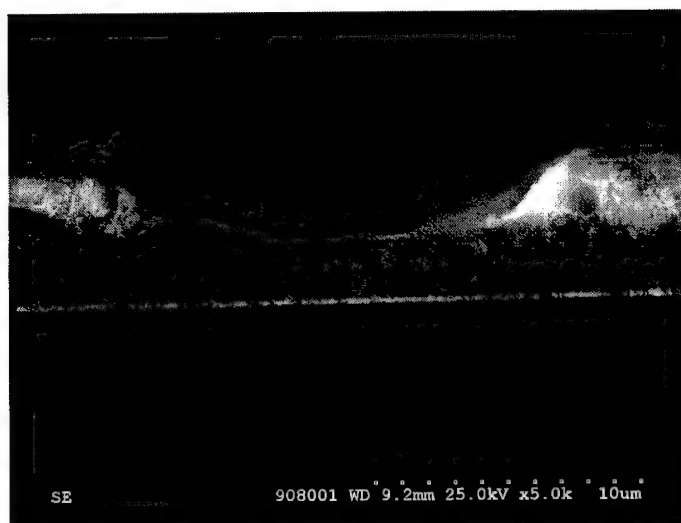
Etching time: 10 min
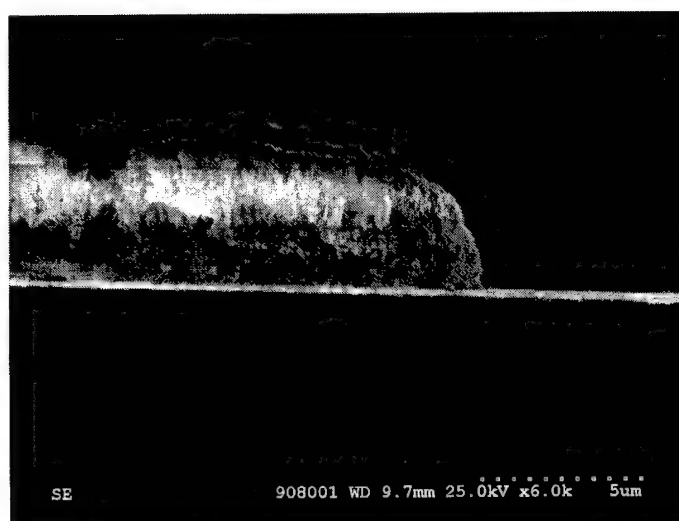
Etching time: 36 min

Figure 14. Etching of PZT film on a Pt substrate with the Draper formula.

Draper formula. In this case, a substrate was being prepared for d_{31} switch configuration. Ultimately it was determined to be most convenient to ion mill both PZT and ZrO_2.

The selection of ZrO_2 as a passivating material is motivated in part by the fact that it can be conveniently derived from the process used to make PZT. An option exists for changing the passivating layer from ZrO_2 to some other thin film. In this case, one would choose a material that could be etched by the Draper formula or similar cocktail. However, this does not appear to be necessary. Ion milling is acceptable for prototype construction, and Northrop Grumman's approach to MEMS production relies on dry etching processes rather than wet etching. As a result, ion milling has been adopted for etching PZT and ZrO_2 as well as metal layers used for electrodes and signal lines (e.g., Au, Cr, Pt).

### 3.2.2 Impact of Interdigitated Electrode Width and Spacing on PZT Strain

There is an implicit trade-off between electrode width and finger spacing in an interdigitated electrode of the type used for d_{33} operations. One would like to place the electrode fingers as close together as is feasible to increase the electric field in the direction parallel to the PZT surface. As noted above, the strain in this d_{33} geometry is more than twice that of the d_{31} configuration. However, when the ratio (finger spacing)/(finger width) = R becomes too small the electric field pattern has a downward bend, which means that it contains a component in the vertical (i.e. d_{31}) direction. Thus, for a given finger width, the finger spacing cannot be too close. It is rather complicated to calculate the optimum finger widths and finger spacings without supplemental experimental data, namely electrode current measured as a function of poling electric field for several different values of R.

The suggested measurements are complicated by the fact that very little current is generated with the electrode potentials appropriate for our system (e.g., ~30 V). The problem is that the current values are very small (pA) and not enough is collected with an interdigitated electrode of the size used for the MEMS switch. The solution is to increase the finger lengths and number of electrodes in order to increase the current while preserving realistic finger widths and finger spacing. To do this, special electrodes had to be generated that were 600×600 microns in size. This required the preparation of separate sets of masks. Three electrode configurations were tested each having a finger spacing of 10 microns.

Figure 15 shows the results of the tests of three different finger widths. The value of d_{31} or d_{33} with transverse electrodes cannot be directly obtained by measuring the piezoelectric current. This is because both the d_{33} and the d_{31} component produce a current contribution and the relative effects are related to the capacitance of the sample. However, by measuring the dependence of the current on poling field, the saturation field can be obtained. By determining the ratio at which the field saturates at the point given by $3E_c = 3 \times 50kV/cm = 150kV/cm$, we can estimate the value of R at which the electric field becomes parallel. On the basis of the current results, the field becomes nearly parallel near R=1.1. These results serve as inputs to a model of the electric field in substrate stack.
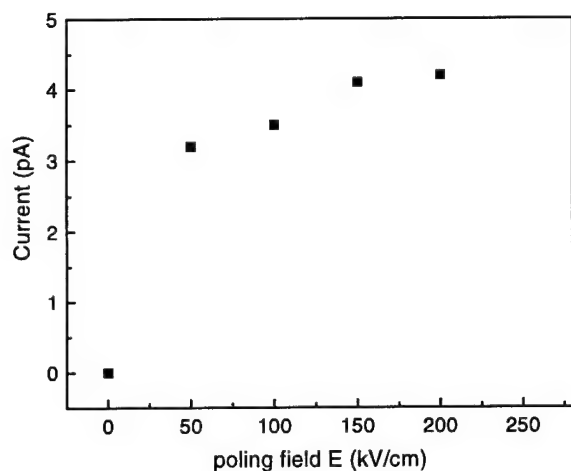
$d_{space} = 10 \ \mu m, \ d_{finger} = \ 3 \ \mu m, \ R=3.3$
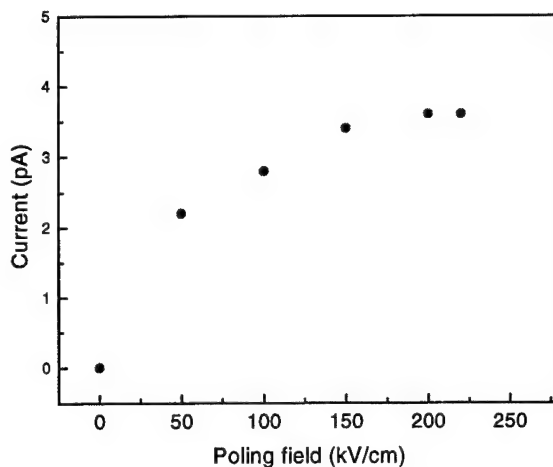
$d_{space} = 10 \ \mu m, \ d_{finger} = \ 9 \ \mu m, \ R=1.1$
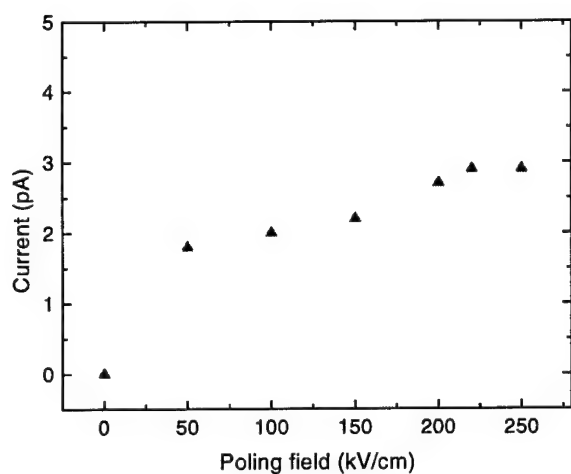
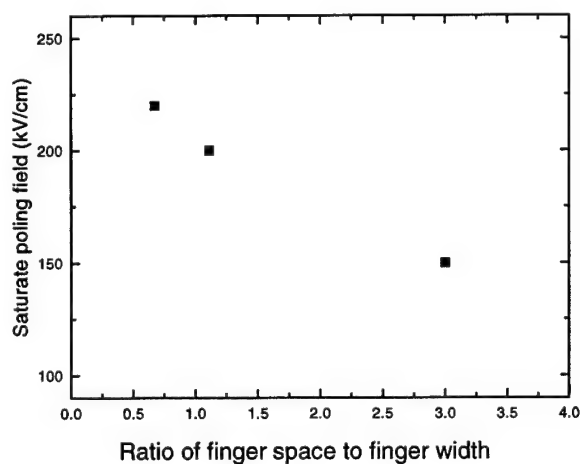$d_{space} = 10 \ \mu m, \ d_{finger} = \ 15 \ \mu m, \ R=0.67$

Figure 15. Dependence of current collected with interdigitated test electrodes versus poling electric field (upper panels and bottom left panel) and the saturation poling field versus the ratio of finger space to finger width, R (bottom, right panel).

4. Cantilever Motion

4.1 Unimorph Cantilever (d_{31})

A unimorph cantilever consists of a single layer of PZT attached either above or below the cantilever substrate (e.g., Si_3N_4). A simplified side-view drawing with the PZT polarization vector **P** pointed upwards is shown in the illustration below. The electrodes that are positioned immediately above and below the PZT layer are not shown in this figure. The absolute direction of **P** is not important for the discussion below; what is important is whether the imposed electric field is parallel or anti-parallel to **P**.
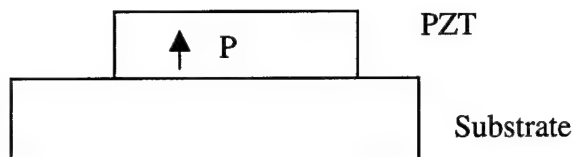
The d_{31} coefficient is negative. As a result, when the applied field E_1 is in the same direction as **P** (parallel to **P**), the PZT contracts, and the cantilever bends upwards. When the applied field E_2 is in the opposite direction (anti-parallel to **P**), the PZT expands and the cantilever bends downwards. However, E_2 must be smaller than the coercive electric field E_c of PZT; otherwise, depolarization of the PZT will occur. If PZT is placed on the bottom of the substrate, the reverse is true, that is, when E_1 is applied parallel to **P** the cantilever would move downwards and when E_2 is applied anti-parallel to **P** the cantilever would move upwards. Thus, the greatest motion upwards occurs with the PZT layer on top of the substrate, and the greatest motion downwards occurs when the PZT is on the bottom.

4.2 Bimorph Cantilever (d_{31})

A bimorph cantilever, which consists of a PZT layer placed above and below the substrate is illustrated below. In this case, when V>0 (E parallel to **P** on the top PZT layer, E
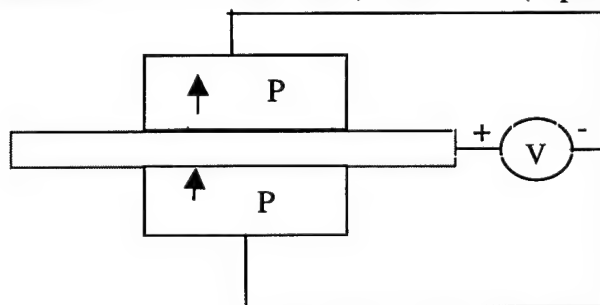
antiparallel to **P** on the bottom PZT layer), the cantilever bends upwards. When V<0, (E antiparallel to **P** on the top PZT layer, E parallel to **P** in the bottom PZT layer), the cantilever will bend downwards. Thus, to make the cantilever bend down or up, the applied field E on one of PZT layers is always antiparallel to its polarization direction. Thus, two different voltages must be used for maximum deflection: one greater than E_c and one less than E_c. If only one voltage is employed as illustrated in the above figure, E must be smaller than E_c.

4.3 Unimorph Cantilever With Interdigitated Electrodes (d_{33})

For d_{33} operations, surface electrodes are used. For convenience, they are generally placed on the top of the PZT layer, which is located on top of the cantilever (see e.g., Figure 2). The top view of the electrodes is shown schematically below. Because the coefficient d_{33} is

24
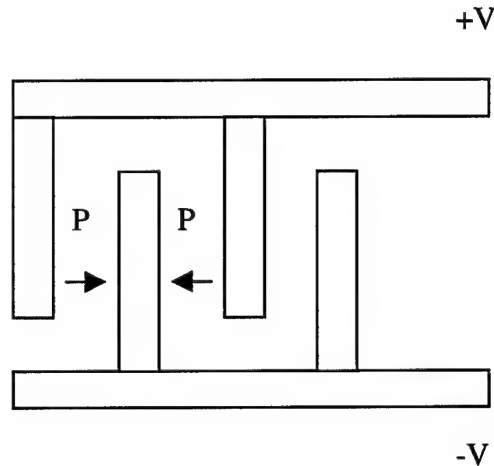
positive, when V>0 (E parallel to **P**), the PZT will expand and the cantilever will bend downwards. When V<0 (E antiparallel to **P**), the PZT will contract, and the cantilever will bend upwards.

5. Microfabrication of MEMS Switches

Initial tests focused on characterizing the movement of the d_{31} cantilever. In this case signal lines and contact electrodes were omitted. The substrate stack consisted of Si/LTO (2 μm SiO$_2$)/Si$_3$N$_4$ (0.4 μm). The bottom (Pt/Ta) electrode was sputtered on the Si$_3$N$_4$, and then PZT was deposited via the sol-gel process. The top Au/Cr electrode was evaporated onto the PZT and patterned by the lift-off technique. PZT and Pt/Ta were patterned into a cantilever-shaped structure using ion milling, whereas the Si$_3$N$_4$ is patterned using RIE. Initially, the ion milling produced ~1 μm roughness on the edge of the cantilever, but this was mitigated by encapsulating the cantilever in 1827 photoresist.

The release process entails the application of HF and Acetone for 2 minutes followed by an IPA rinse. The cantilevers are to be placed in a warm IPA bath. A hot plate is then set to 85 C, and the IPA is allowed to evaporate. The yield of free standing cantilevers is about 95%.

Figure 16 provides an example of motion of the d_{31} cantilever. A sinusoidal voltage ranging from 0 to 14 Volts is applied to the electrode. Three frames from a "movie" are shown in Figure 16. The cantilever starts at the electrode level (top of figure) and then increases in height by about 3 μm. The resonance speed obtained for the cantilever corresponds to 2 μm closure time of about 10 μs, which is consistent with the theoretical expectations for a cantilever 200 μm in length and a thickness of about 2 μm.

As noted in Section 4, a d_{31} cantilever with the PZT on top of the Si$_3$N$_4$ will have the greatest displacement if voltage is applied to the electrodes in the poling direction. In this case, the cantilever will move upwards as illustrated in Figure 16. When the electrodes of Figure 16 were driven antiparallel to the poling direction, the maximum voltage that could be applied without depoling the PZT was about –5 V. This resulted in a smaller (~1 μm) downward displacement. The –5 V generated an electric field strength near the coercive electric field of the PZT. When higher reverse voltages were applied, the PZT depolarized as expected.
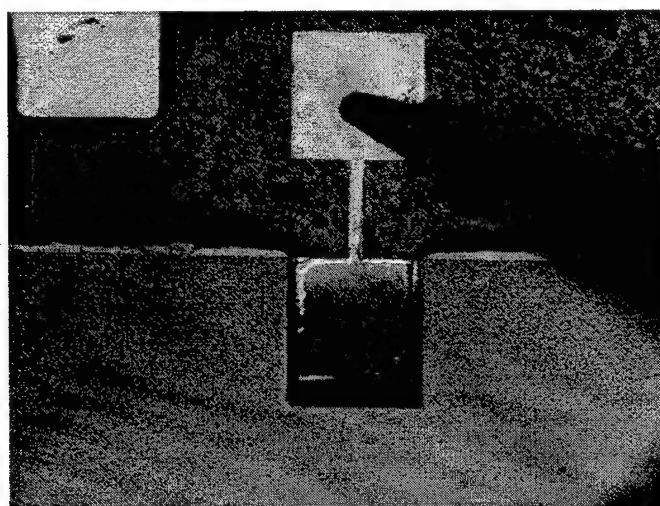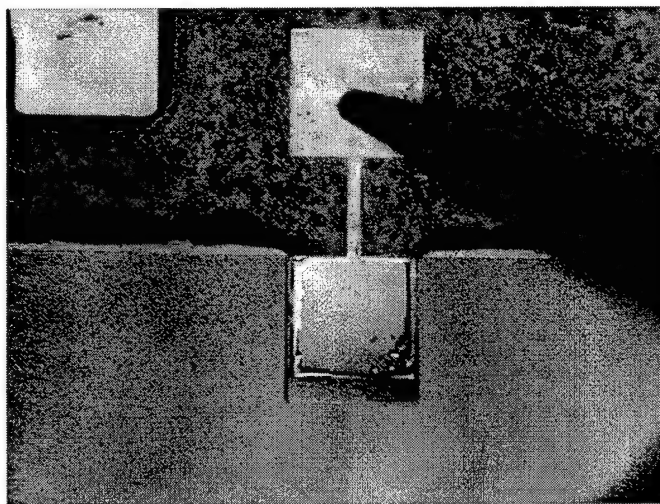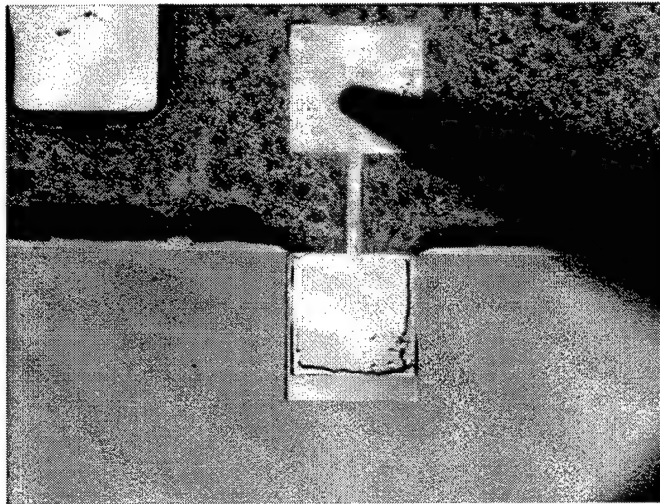
25

Figure 16. Motion of a d31 cantilever observed in reponse to a 0-14
volt electrode source that was sinusoidally varied at a
period of ten seconds. The displacement is approximately
3 microns. The size of the cantilever structure is 250 microns
by 200 microns.

26

A downward moving switch with optimum displacement requires that the Si_3N_4 be placed above the PZT (e.g., Figure 1) rather than below it as was the case in the above tests. The PZT was placed above the Si_3N_4 because it is most expedient to do so from a fabrication standpoint. There are two strategies that can be employed to place the layer of low stress Si_3N_4 above the PZT layer. First, one can invoke a fabrication sequence that involves LPCVD (at 700 C) of Si_3N_4 on the cantilever stack containing PZT. Although many foundries will not accept this task because of the lead in PZT, a machine capable of doing this is currently in operation at Penn State. Unfortunately, attempts to build a downward moving d_{31} switch during the Phase 1 period were hampered by delays in bringing a LPCVD Si_3N_4 machine on-line. The operation of this unit was not directly controlled by any member of the GRI/PSU team. A second methodology for placing the Si_3N_4 above the PZT layer is by developing a cantilever stack similar to that tested above and then flipping the stack 180 degrees and bonding it to a low-k substrate. A wafer bonding machine was not available at PSU during the Phase 1 project. However, one has been ordered (Electronic Vision Corporation Model 501), and this unit is expected to be received and placed into service by July 2001.

In light of the project resources available in December 2000/January 2001, attempts were made to construct an upwardly moving d_{31} MEMS switch. The fabrication sequence for this switch is illustrated on pages 28-30 below. The principal difficulty with this approach is the construction of a level platform for the transmission lines above the cantilever. Three frames from a "movie" showing motion of the cantilever used to close the switch are presented in Figure 17. The contact on the cantilever did not succeed in closing the switch. Additional investigations indicated that the problem was that the transmission lines were tilted out of plane relative to the signal contact on the cantilever. We concluded that this type of upward-moving d_{31} switch was very difficult to fabricate, and that other approaches needed to be examined. As noted above, one can employ either LPCVD of Si_3N_4 on PZT or use wafer-bonding techniques for the classic downward moving switch. The latter appears to be most promising from a fabrication point of view and eliminates the need for special purpose LPCVD equipment. The suggested d_{31} switch fabrication involving wafer bonding is illustrated on pages 32-34 below.

In addition to the d_{31} studies, test cantilevers were formed for operation in d_{33} mode. In this case, we started with a substrate stack of Si/LTO(SiO_2)/low stress Si_3N_4 (ordered from bottom to top). The layers ZrO_2/PZT/interdigitated electrodes were subsequently deposited on top of the Si_3N_4 layer. The interdgitated electrode consists of Au/Cr, which is evaporated onto the PZT and patterned via the lift-off process. The top view of a d_{33} cantilever is displayed in Figure 18 below. This figure illustrates the general pattern of interdigitated electrodes. In this particular case, the finger width of the interdigitated electrode is 6 μm and the gap between electrodes is 3 μm. During the d_{33} tests, the best combination was found to be finger width = 3 μm and gap width = 3 μm.
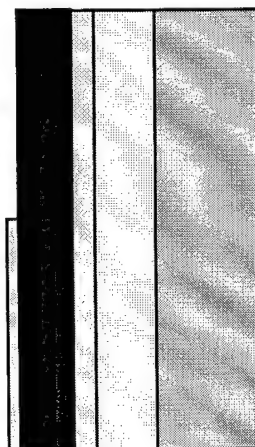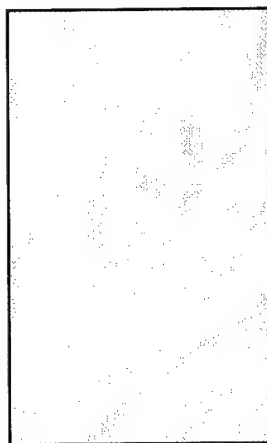
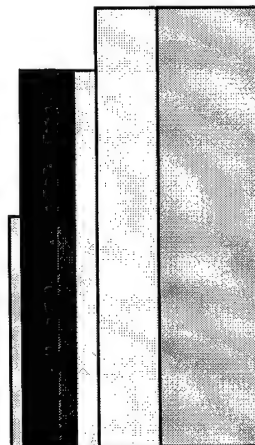Figure 18. Top view of the interdigitated electrodes subsequent to the definition of the cantilever by ion milling.
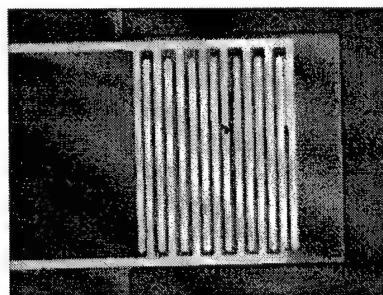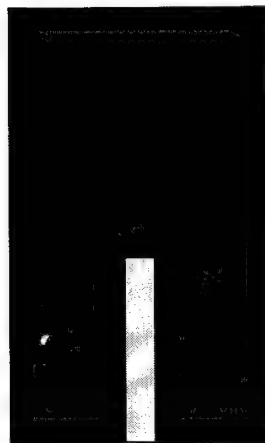
# Fabrication flow processes for a d_{31} upward moving switch

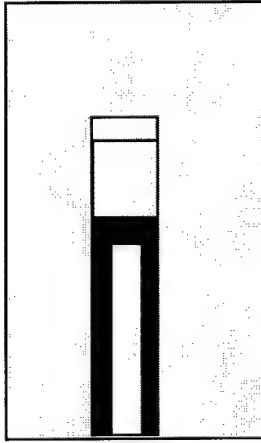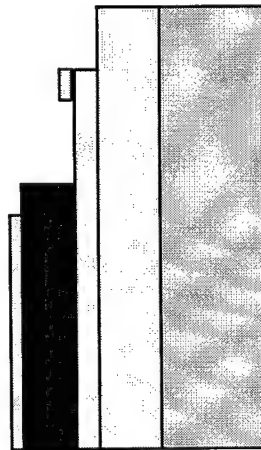1. Silicon wafer with 2 μm sacrificial oxide layer and 0.4 μm low stress Si_3N_4.

2. Bottom Pt/Ta electrode is sputtered on Si_3N_4, and then PZT is deposited by sol-gel technique. The top Au/Cr electrode is evaporated on PZT and patterned by lift-off.
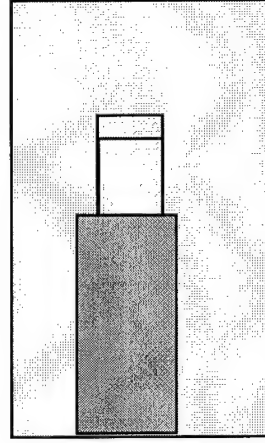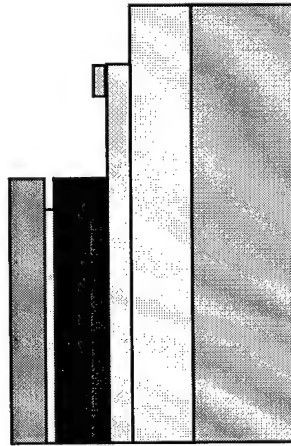
3. PZT and Pt/Ta are patterned into a cantilever shaped structure using ion-milling and Si_3N_4 is patterned using RIE.
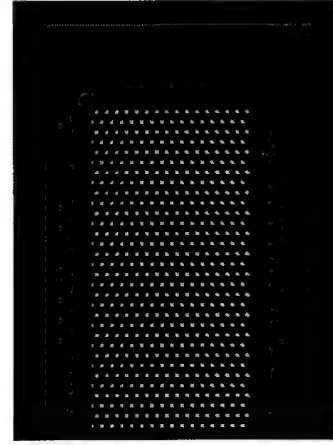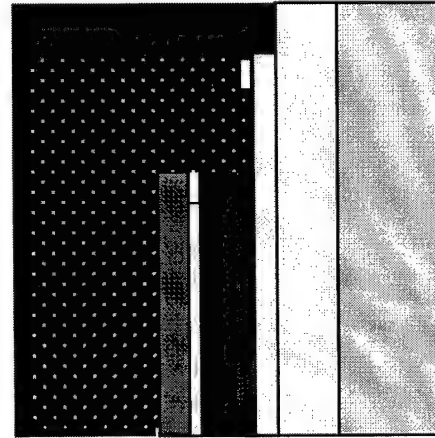

28
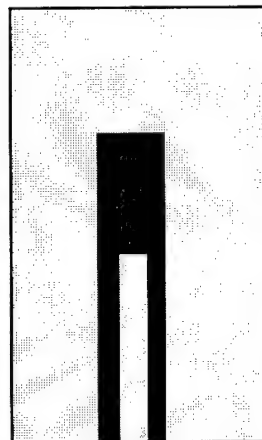
4. PZT at the end of cantilever is wet etched in HF and Pt/Ta below the PZT is etched by ion milling. Then the contacted bottom Au/Cr is formed on the appeared Si_3N_4 by lift-off.


5. Two layers of 1811 photoresist are spin coated on the top and patterned by encapsulation mask, following by hard bake at 155°C for 10 min.

6. A layer of thick photoresist (SJR5740) is deposited and area above the cantilever is exposed (no develop) with the "window" mask. Then Au/Cr is sputtered on the whole surface.

29
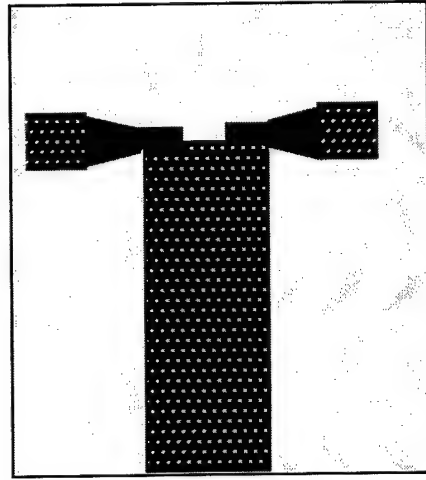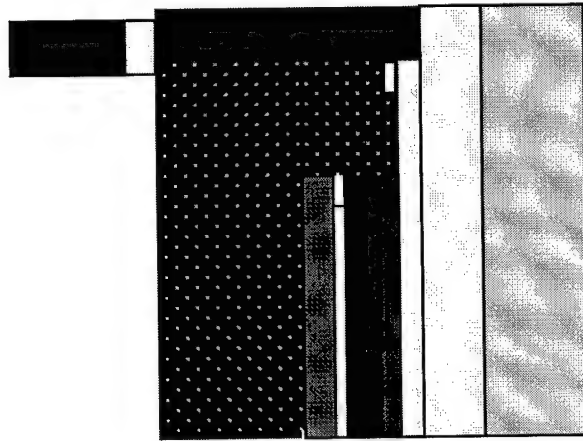
7. After Au/Cr is sputtered on the whole surface, another layer of SJR5740 photoresist is spin coated on the Au/Cr and patterned into transmission line by wet etch Au/Cr. Then the photoresist in the area of the transmission pad is exposed again.
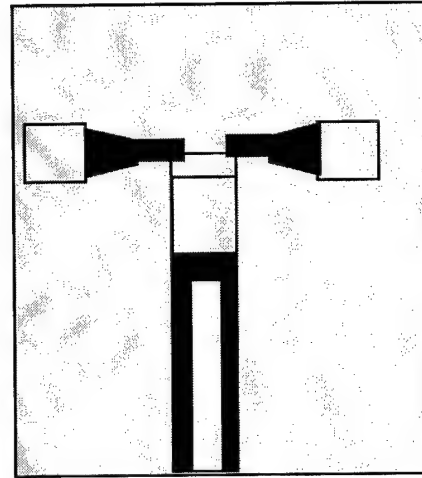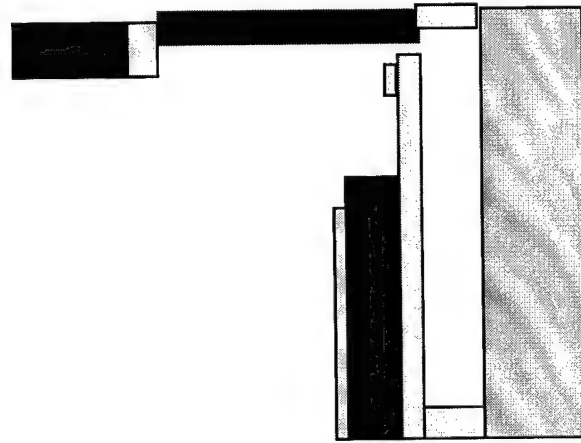
8. Develop exposed photoresist and then release the cantilever in HF mixture. Finally, remove photoresist on the cantilever by O$_2$ plasma.
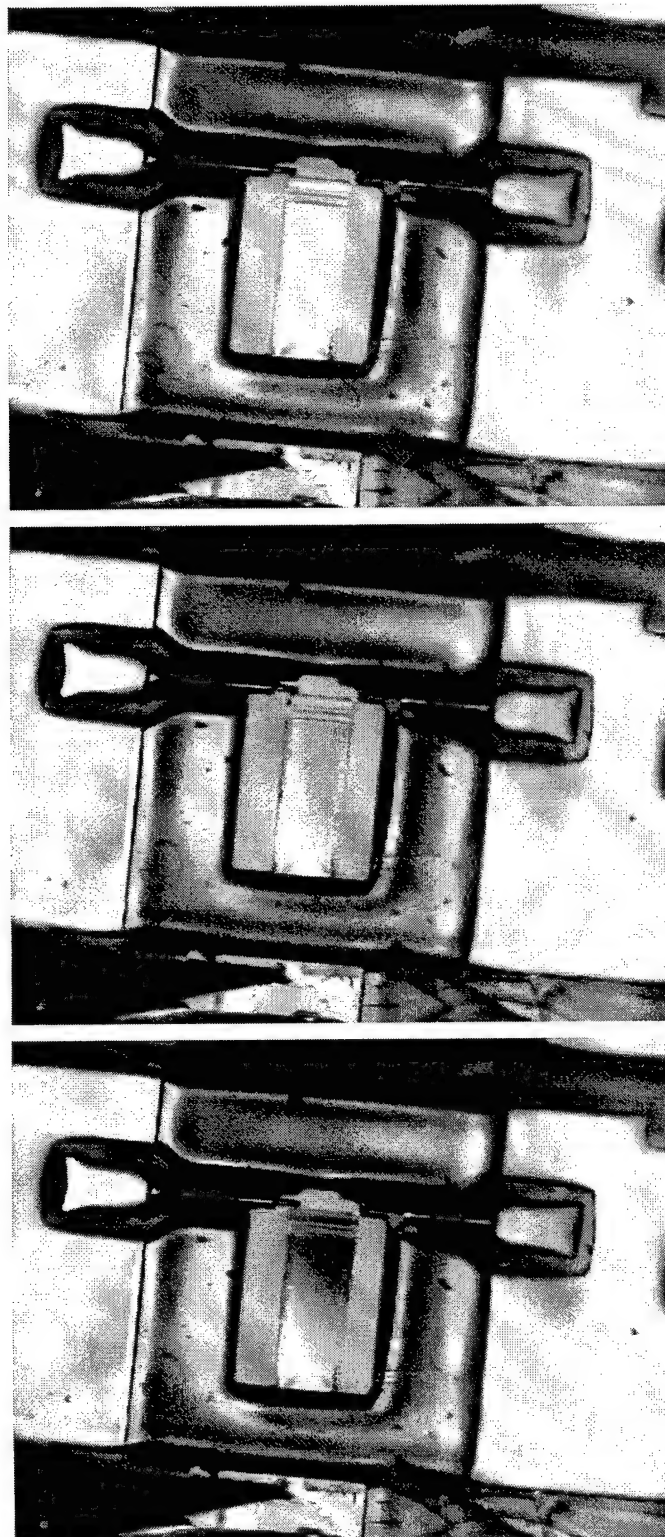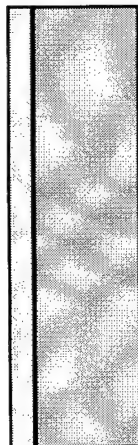
Figure 17. Motion of an upward moving d31 switch in response to a 0-14 volt
source that was sinusoidally varied at a period of ten seconds. The
size of the cantilever structure is 150 microns by 50 microns.

Fabrication flow processes for a d_{31} downward moving switch

1. Silicon wafer with 0.4 μm low stress Si_3N_4.
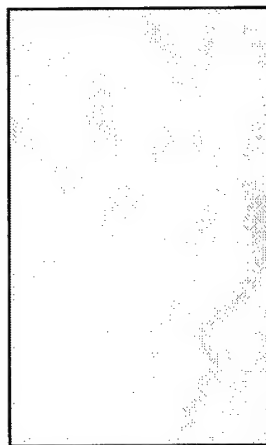
2. Bottom Pt/Ta electrode is sputtered on Si_3N_4, and then PZT is deposited by the sol-gel technique. The top Au/Cr electrode is evaporated on PZT and patterned by lift-off.
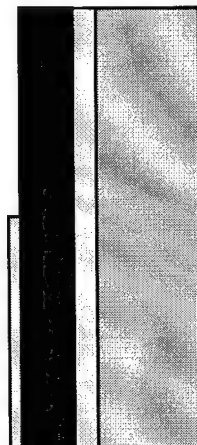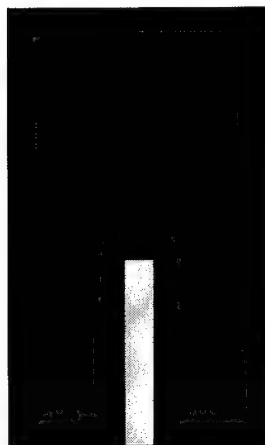
3. PZT and Pt/Ta are patterned into a cantilever shaped structure using ion-milling, and Si_3N_4 is patterned using RIE

32
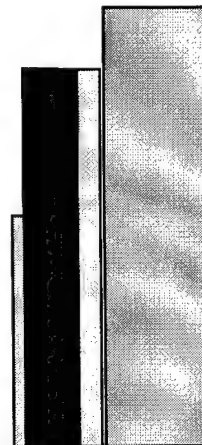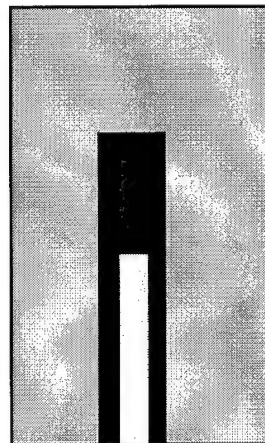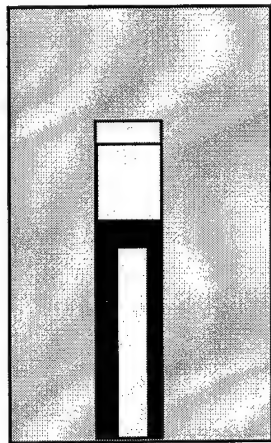
4. PZT at the end of cantilever is wet etched in HF and Pt/Ta below the PZT is etched by ion milling. The contact Au/Cr electrode is then formed on the exposed Si_3N_4 by the lift-off process.
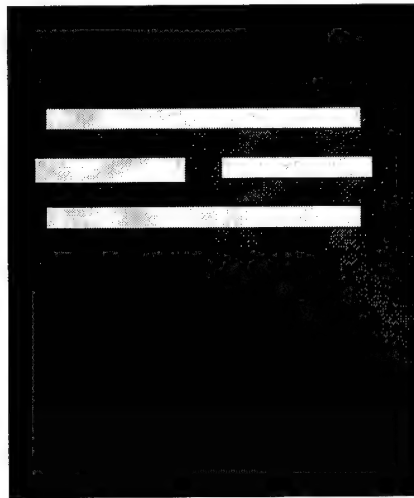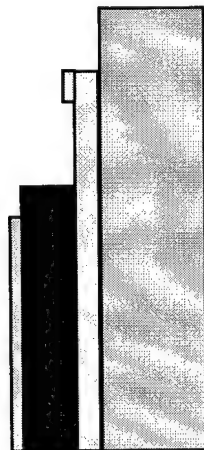
5. Deposit Au/Cr transmission lines on a low k ceramic substrate.

33
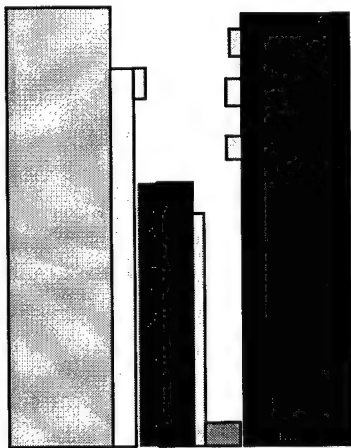
6. The stacked structure is turned upside down and is bonded onto the ceramic substrate.
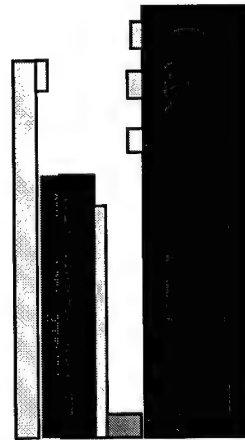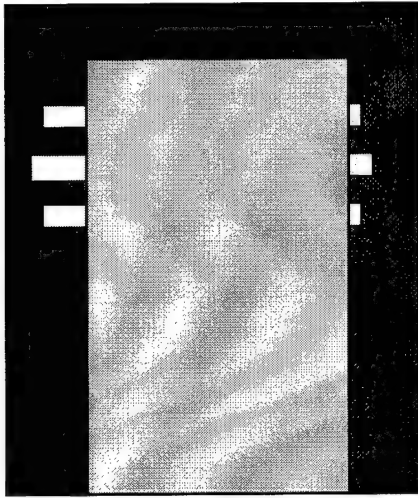
7. Finally, the silicon is etched by Deep Reactive Ion Etching (DRIE).

34
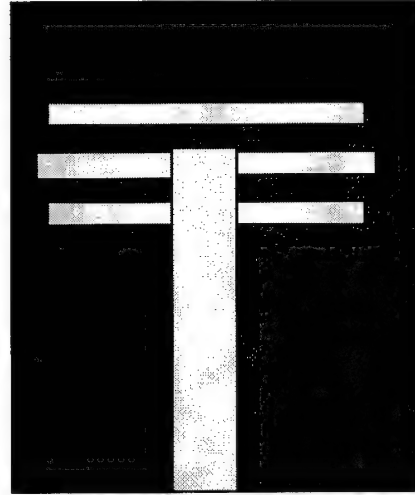
The PZT/ZrO$_2$ was patterned into a cantilever using ion milling, and the photoresist was subsequently removed with an O$_2$ plasma. The PZT/ZrO$_2$ is subsequently encapsulated with photoresist (1827), and RIE is used to pattern the Si$_3$N$_4$. The cantilever is released by etching the LTO in HF.

Three frames from a "movie" showing ~1 μm motion of the cantilever are presented in Figure 19. A maximum of 10 volts was applied to the electrodes. The cantilever displacement scales roughly linearly with applied voltage.

The methodology for fabricating a d$_{33}$ cantilever switch is illustrated in pages 37-39 below. It was not possible to build this switch during Phase 1 owing to the fact that PSU's LPCVD Si$_3$N$_4$ machine was not operational at the time. Nevertheless, the cantilever tests provide the most important insight into utility of the d$_{33}$ configuration. It requires approximately twice the voltage of the d$_{31}$ configuration for a similar cantilever displacement.

6. Trade-Offs Between d$_{31}$ and d$_{33}$ Switch Operation

Although the d$_{33}$ mode has slightly more than twice the strain of the d$_{31}$, it may not be as effective as the d$_{31}$ mode in certain cases. The reason for this is that it is more difficult to achieve high electric fields in the PZT with the interdigitated electrode arrangement. In addition, the percentage of active PZT space is reduced by the surface space occupied by the electrodes. To illustrate this effect, we set the finger width at the smallest value acceptable for fabrication (2 microns). One can then calculate the applied voltage required to generate a reasonable electric field in the PZT (250 kV/cm). Figure 20a shows the applied voltage required to maintain 250 kV/cm versus electrode spacing, and Figure 20b illustrates the strain that can be developed versus electrode spacing. To achieve a reasonable strain value (1.5×10^{-3}), a spacing of 3 μm is required. This in turn requires an electrode voltage of 90 V.

The above electrode voltage can be compared to that required to generate a similar amount of strain in the d$_{31}$ mode. Here we assume that the PZT layer thickness is 1 μm. The required voltage for a strain of 1.5×10^{-3} is readily calculated to be 50 V. Thus less electrode voltage is required to operate in the d$_{31}$ mode. This can be a significant advantage. However, the shortcoming of the d$_{31}$ mode is that the required value of the electric field in the PZT (~500 kV/cm) is potentially near the breakdown limit of the PZT. This limit depends not only on the electric field level but the duty cycle of the electric field as applied to the PZT. For a continuous application of an electric field, the breakdown voltage typically ranges from ~500 kV/cm to 1 MV/cm. Device lifetime in PZT thin films is typically limited by resistance degradation and/or time dependent dielectric breakdown (TDDB) [8,9]. It has been shown that although both types of breakdown involve the slow increase in the leakage current with time during dc operation, different mechanisms can be responsible for the failure [9]. In essence, TDDB is destructive and causes the capacitor formed by the electrodes to short, while resistance degradation is associated with an increased current density that does not necessarily cause breakdown [9]. The leading cause of resistance degradation in acceptor doped titanates is oxygen vacancy migration [10,11]. During operation, oxygen vacancies begin to pile up near the cathode creating a region of n-type conductivity. This leads to a depletion of oxygen vacancies near the anode resulting in a region of p-type conductivity. In turn, this yields a forward biased pn junction in which the leakage current continues to rise until breakdown.

35
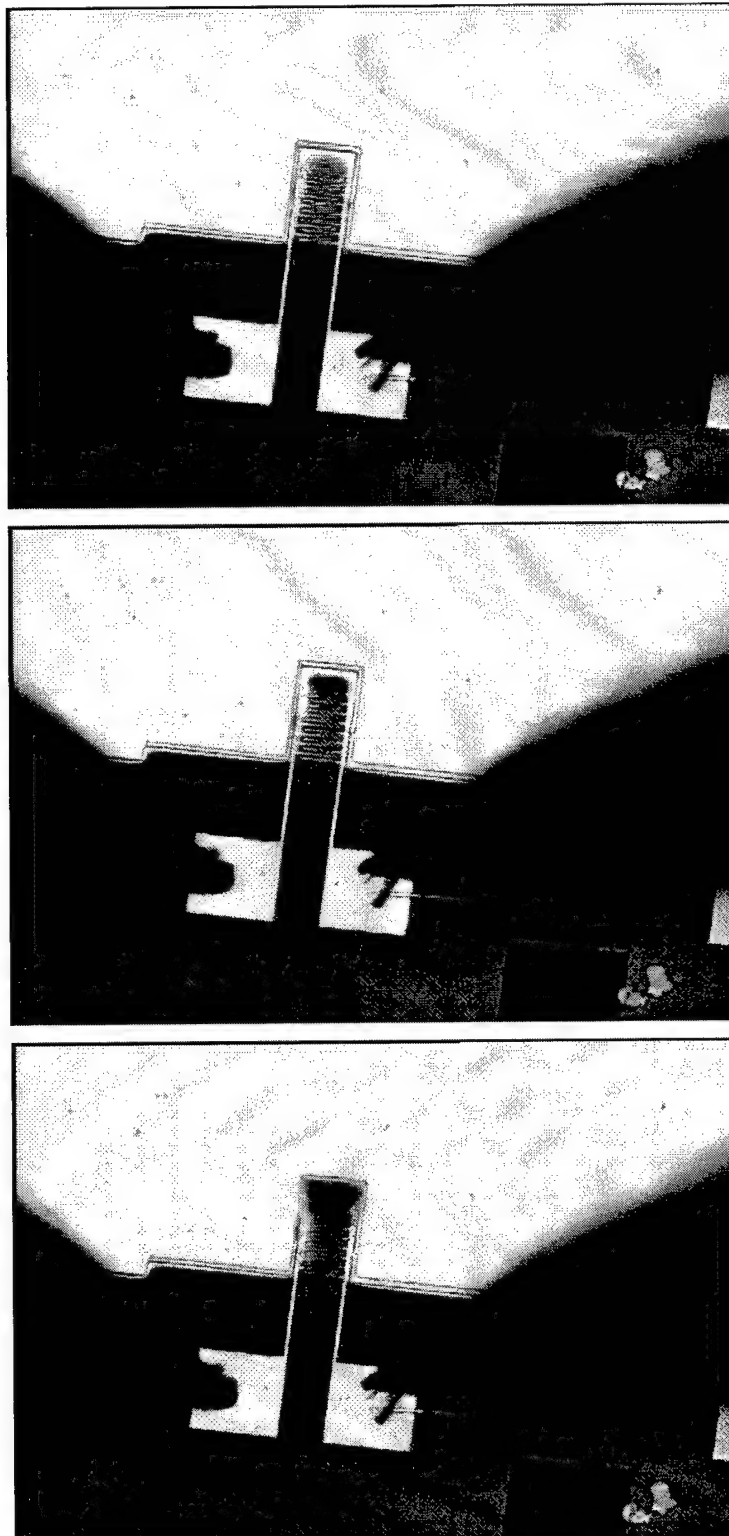
Figure 19.   Motion of a d33 cantilever observed in reponse to a 0-10
volt electrode source that was sinusoidally varied at a period
of ten seconds.The size of the cantilever is 200 microns by 100 microns

36

**Fabrication flow processes for a d_{33} downward moving switch**
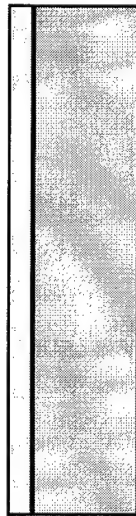
1. Silicon wafer with a thin Si_3N_4 insulating layer.
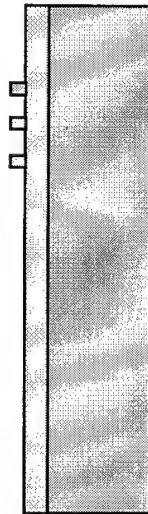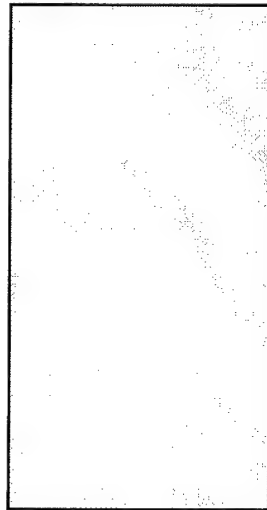
2. Au/Cr transmission lines are deposited on Si_3N_4.
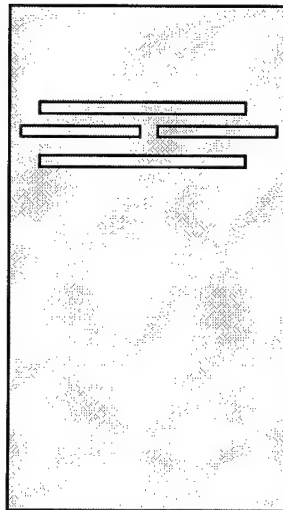
3. Low temperature oxide (LTO) is deposited for use as a sacrificial layer.

37
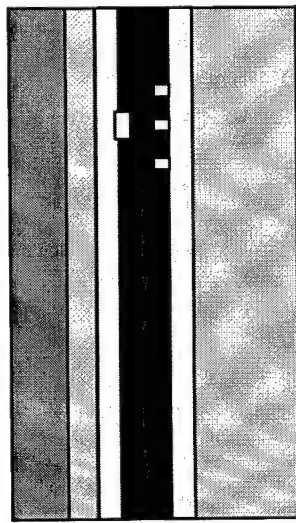
4. After depositing the contact electrode, a layer of low stress Si_3N_4 is deposited as structural material for the cantilever. Then the ZrO_2 buffer layer and the piezoelectric PZT layer are deposited by the sol-gel method.
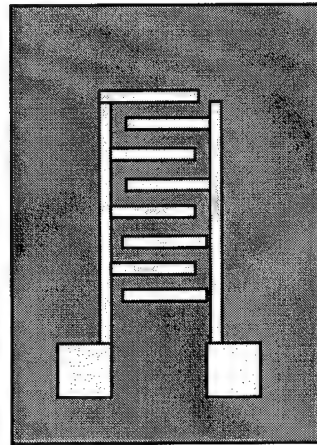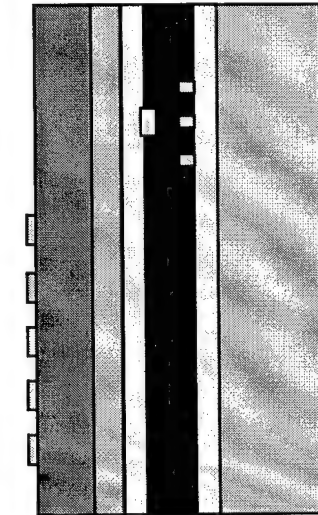
5. The top interdigitated Au/Cr electrode is evaporated on PZT and patterned by lift-off.
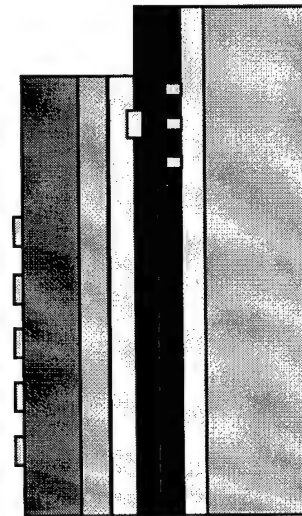
6. PZT and ZrO_2 are patterned into a cantilever shaped structure using ion-milling, and Si_3N_4 is patterned using RIE.

38
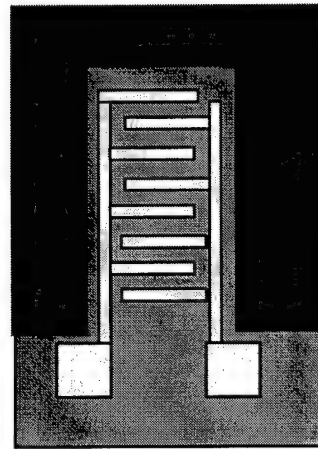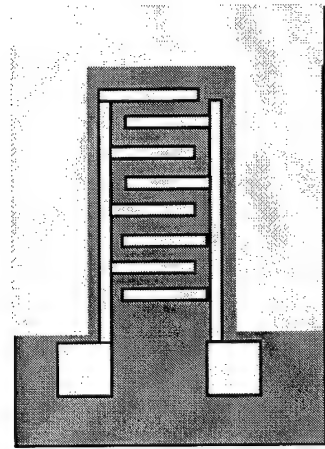
7. A encapsulation mask is used, and the cantilever is released by etching the LTO in HF.
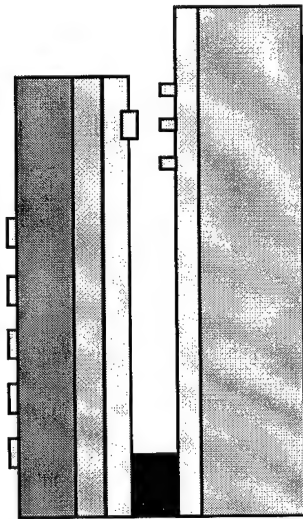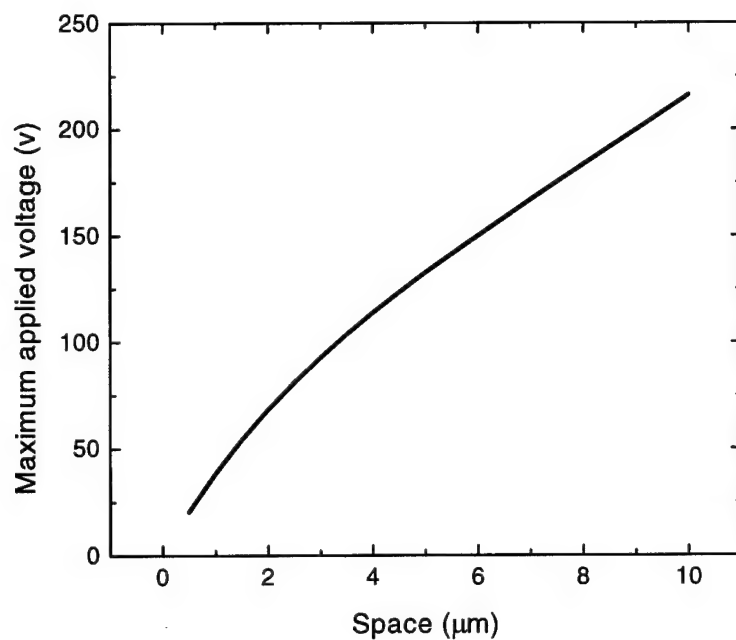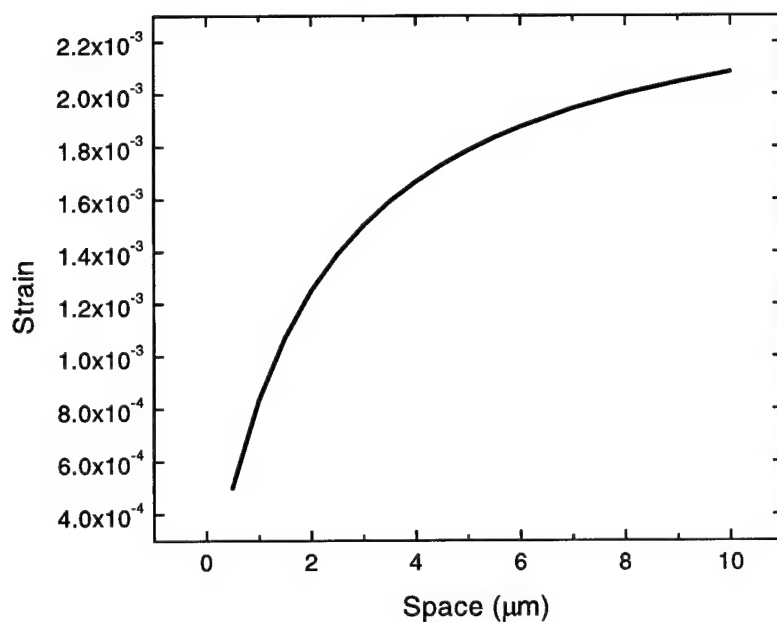
Figure 20.   Maximum applied voltage required to generate a d_{33} electric field of 250 kV/cm for a finger width of 2 μm versus space between electrodes (upper panel), and d_{33} strain versus electrode spacing (lower panel).

At an electric field of 1 MV/cm, one expects the migration of the finite number of oxygen vacancies to lead to the destruction of the piezoelectric properties of PZT. The time constant for breakdown tends to be of the order of 1-2 minutes for a continuously applied electric field. The symptoms are a rapid increase in the leakage current at the electrodes and/or spikes in the electrode current caused by damaged PZT regions. Ultimately, electrode melt down occurs. One can significantly increase the breakdown threshold voltage of PZT with the aid of donor doping techniques, but this has not been explored as part of the Phase 1 project.

If there were no restrictions on voltage, then the d_{33} mode could be used to generate more strain than that available with d_{31}. For example, a strain value of 3.0×10^{-3} can be achieved with a voltage of 180 V. At the same time, the PZT would remain in a safe electric field zone.

Overall, the Phase 1 strategy of constructing a (slow) cantilever switch served its purpose in that it led to the validation of PZT as an actuator for MEMS RF switches. In addition, it allowed the GRI/Penn State team to gain experience in fabricating micro-devices with PZT and led to the development of a knowledge base required for the design of very fast RF switches in Phase 2.

7. Other Recent Developments in PZT MEMS Switches

In the past, the operation of a piezoelectric cantilever for force-sensing applications has been discussed in the literature [12]. More recently, the construction of a PZT-based MEMS microwave switch has been reported by Marconi Caswell Ltd. [13]. The PZT layer was deposited using the sol-gel process. Cantilever release was achieved using a combination of bulk silicon etching and deep reactive ion etching with a STS Multiplex system.

The speed of the Marconi Caswell switch (tens of μs) is much slower than that required by the current program. Nevertheless, the characteristics and design of the switch are of interest. The switch structure is flip-chip bonded onto a substrate with ground and signal lines in either a microstrip or coplanar layout. Flip-chip bonding was employed to allow the switch to be placed on most substrates. Placement accuracy of the switch above the signal lines was $\pm$ 2 μm in the x-y directions and $\pm$ 0.5 μm in the z direction. The actuated cantilever opens and closes a gap in the signal line. A clearance of 2 μm above the signal line when open provides 25 dB isolation at 50 GHz with the isolation increasing as the frequency decreases. A gold pad at the end of the cantilever acts to close the gap of 100 μm in the signal line.

The program proposed here is far more complex than that described in [13] because the required switching speeds are more than 1000 times greater than those implemented by Marconi Caswell. This forces us to probe the technological limits of the materials and processes used to construct the switch.

8. Design Strategies for a High-Speed MEMS Switch

Three approaches for the development of very high speed MEMS switches were developed as part of the Phase 1 effort. They consist of a bimorph cantilever design, piezoelectric extensional bars, and a flextensional "moonie" actuator. In addition, it is possible to combine the bimorph cantilever with the flextensional actuator to provide superior signal isolation in the RF switch off state.

None of the systems described below have been optimized and detailed modeling has not yet been performed. The strategies discussed below can be considered to be part of our "tool set" for speeding up MEMS switches well beyond any that have been constructed to date.

8.1 Bimorph Cantilever

The bimorph cantilever consists of two PZT thin films separated by a middle layer often used to add stiffness to the cantilever. When an electric field is applied to bimorphs, one of the PZT layers expands (top layer), and the other contracts (bottom layer). This mechanism creates a bending displacement that is significantly better than a unimorph. In the design of the actuator, the characteristic parameters of primary concern are resonance frequency, tip deflection and generative force. The lowest mechanical resonance frequency determines how fast the switch can turn on, tip deflection impacts switch isolation, and generative force determines, in part, contact resistance. There are trade-offs among each of the above parameters, and one seeks to optimize the parameters for a specific application.

For our approximate analyses, we will assume that the bimorph middle layer is composed of Si_3N_4, giving rise to a PZT/ Si_3N_4/PZT stack. Other layers necessary for fabrication (e.g, metallic layers for electrodes and ZrO_2 buffer layers) are omitted because they do not have a major impact on the results. For a cantilever structure having uniform mass per unit length, one can then characterize a bimorph actuator using the following approximate analytic equations [3]:

$$\delta = (3L^2/2t)\ \Gamma\ d_{31}\ E_3 , \qquad (1)$$

where δ is tip deflection, L is the length of the cantilever, d_{31} is the piezoelectric coefficient of the PZT layer driven by an electric field E_3 perpendicular to the surface, and

$$\Gamma = (1+B)(2B+1)/(AB^3+3B^2+3B+1), \qquad (2)$$

$$A = E_{SIN}/E_{PZT},\ B = t_{SIN}/2t_{PZT},\ t = t_{SIN}+2t_{PZT}, \qquad (3)$$

where t is total layer thickness and E is Young's Modulus.

Similarly, one can express the resonance frequency as:

$$f_r = 3.52\ t\ (E_{PZT}/3\rho_{PZT})^{1/2} \cdot \Phi/4\pi L^2, \qquad (4)$$

$$\Phi = [1+3(1+2B)^2+4AB^3]]^{1/2}/[4(1+BC)(1+B)^2]^{1/2}, \qquad (5)$$

where ρ is mass density, and $C = \rho_{SiN}/\rho_{PZT}$.

Finally, the blocking force can be expressed as:

$$F_b = (3wt^2E_{PZT}/8L) \cdot \Omega \cdot d_{31} \cdot E_3, \qquad (6)$$

$$\Omega = (2B+1)/(B+1)^2, \qquad (7)$$

where w is cantilever width.

The parameters that are applicable to the present calculations are

Young's Modulus: $E_{PZT} = 101$ GPa, $E_{SiN} = 270$ Gpa

Mass Density: $\rho_{PZT} = 7400$ kg/m^3, $\rho_{SiN} = 3200$ kg/m^3,

We have not attempted to optimize all aspects of the bimorph, but we can quickly determine whether it is feasible. Figures 21a, 21b, and 21c show the calculated results for various values of L/t. It is clear that for f_r to be high, the cantilever length must be short. A comparison of resonance frequency between the bimorph and unimorph cantilevers is provided in Figure 21d. Let us set L = 50 μm and use a cantilever width of 20 μm. The thicknesses of the cantilever layers are selected as 3.2 μm for the PZT and 3.6 μm for the Si$_3$N$_4$. Finally, we set E$_3$ = 50 V. This yields a value for tip displacement of 0.7 μm and a resonant frequency of ~3 MHz, which corresponds to a 10 to 90% rise time of 96 ns. These values are favorable, but we would still like to improve each one of them.

The tip displacement can be doubled using a dual cantilever arrangement shown in Figure 22. This automatically generates a contact to contact separation of 1.4 μm. Nevertheless, we would like to further improve this separation if possible. If we could reverse bias the cantilever electrodes at a voltage near 5 V when the switch is off, the contact separation would improve to about 1.54 μm. In general, the reverse biasing of the electrodes should never exceed the coercive field strength (~50 kV/cm) of the PZT. Special poling methods described in Section 3.1 to mitigate the PZT aging effect would also serve to increase the coercive field. Additional improvements could be made by sputtering the PZT rather than using the sol-gel process. Still another method that can be used to increase tip deflection is to taper the cantilever thickness near the end of the cantilever. However, we have not examined this option in great detail at the time of this writing. Finally, tip displacement can also be improved by optimizing the relative layer widths of the PZT and the Si$_3$N$_4$. Our values of 3.2 μm for the PZT and 3.6 μm for the Si$_3$N$_4$ were used because they appeared to be reasonable.

The time constant of the switch can readily be decreased from 96 ns to 46 ns by using a triangular shaped cantilever instead of the rectangular one (20 μm wide × 50 μm long) adopted for the analyses above. In this case the width of the cantilever near its anchor would increase to 50 μm, but the length would be preserved at 50 μm. In so doing, one would reduce the blocking force somewhat, but this impact is small because the value of F_b/w (250 N/m) is already very high.

As noted above, we have not performed an optimized study of the bimorph, but it is clear that reasonably good actuator characteristics can be achieved with little effort. The simplest way of improving both the tip deflection and resonance frequency is by using a center material that has a greater E/ρ ratio than Si$_3$N$_4$. In addition, one can add a flextensional metal cap as the bottom contact of the bimorph to greatly improve switch isolation. This is discussed in greater detail in Sections 8.3 and 8.4 below.
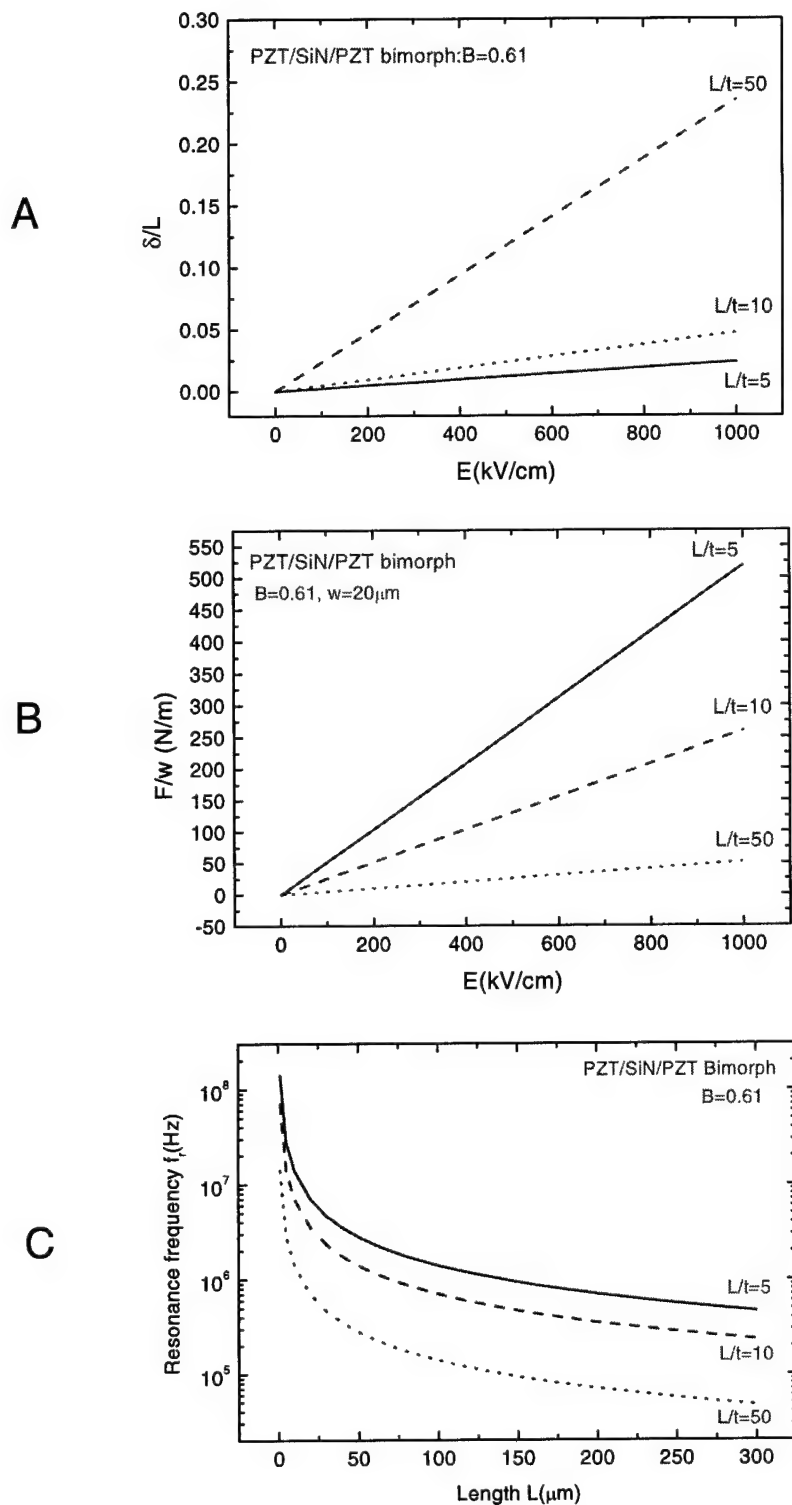
Figure 21.   Calculated results for a bimorph arrangement. (a) Displacement expressed in units of cantilever length versus d_{31} electric field, (b) blocking force per unit width versus d_{31} electric field, (c) resonance frequency versus cantilever length for three length-to-thickness (L/t) ratios.
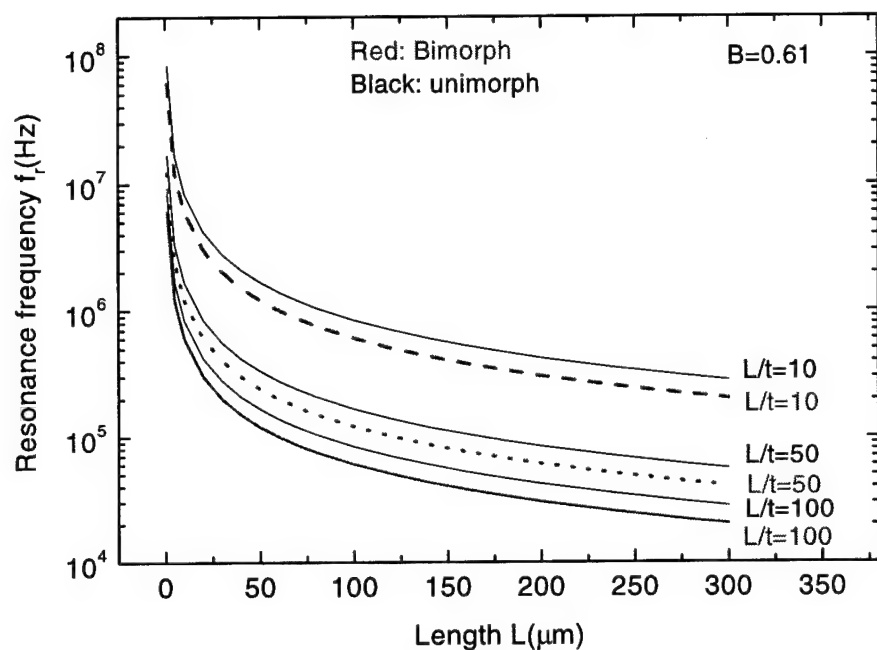
Figure 21d. Comparison of resonance frequencies for a bimorph and unimorph cantilever.
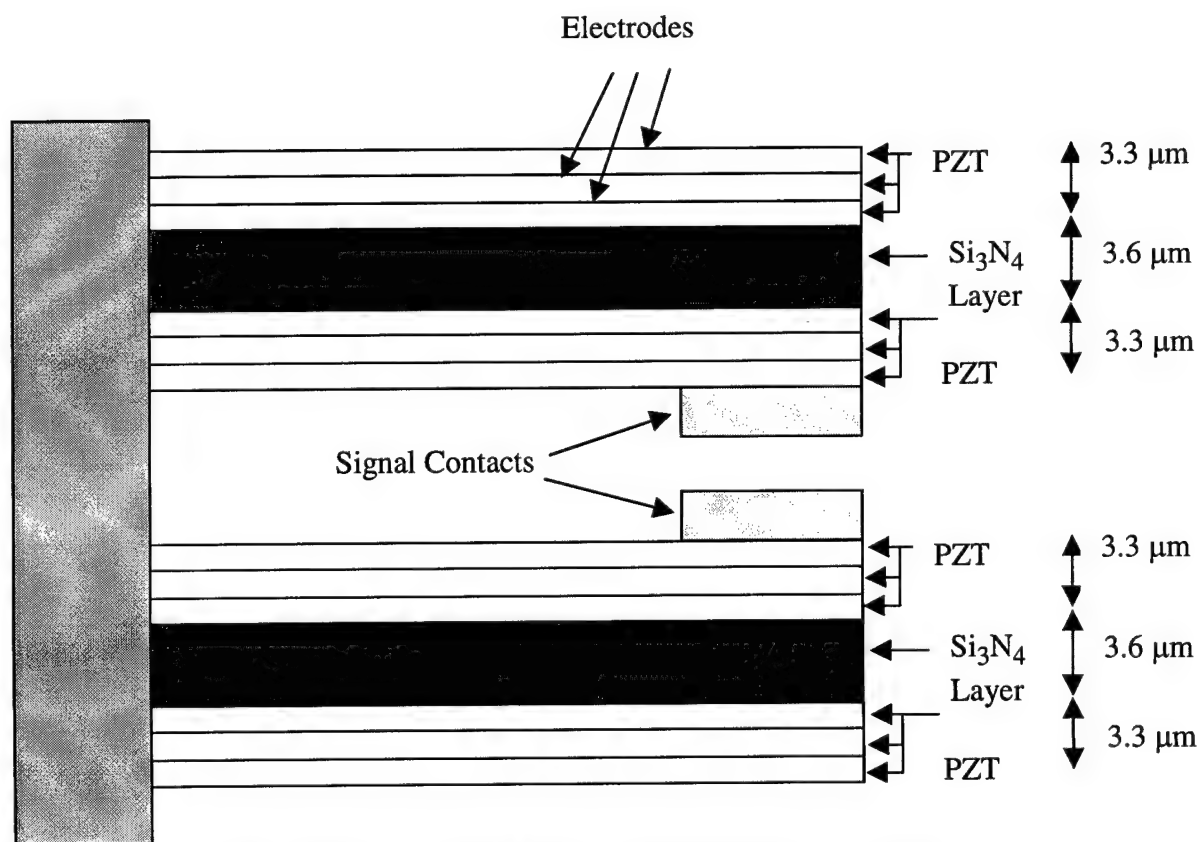
Figure 22. Two bimorph cantilevers stacked with contacts facing one another.

45

8.2 Piezoelectric Extensional Bars

A second approach that will be investigated for the high-speed switch is a series of cascaded length extensional piezoelectric bars. As shown in Figure 23 below, a short length (~ 100 μm) of an end-supported actuator material will be driven so that it expands along its

Figure 23. Schematic of length extensional switch
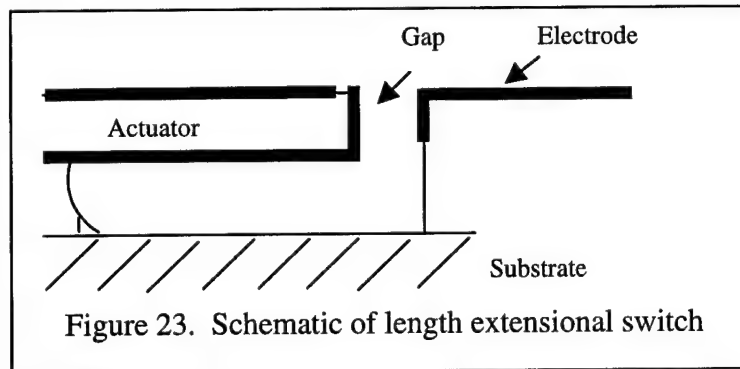
length to close a contact. Because individual elements may have an end displacement ≤ 1 μm, several such switches might have to be placed in a series to achieve sufficient isolation. The response speed of the actuator should be limited by the longitudinal frequency constant (proportional to the velocity of sound) of the material, which is on the order of 1300 to 4000 m/s in the lead-based perovskite materials being considered here. Several approaches will be considered in order to maximize the lateral displacements in one stage of the switch. First, lead zirconate titanate (PZT) films will be investigated. A number of papers have predicted that once the PZT films are freed from the constraints imposed by the underlying substrate (as proposed here), the effective piezoelectric coefficients may nearly double [15,16]. It may also be possible to donor dope the free-standing films to facilitate extensive contributions to the piezoelectric effect (via motion of the non −180° domain walls). The latter leads to another doubling of the room temperature piezoelectric response in bulk PZT ceramics [17]. To date, however, this contribution has been heavily clamped in thin films measured on rigid substrates [16,19]. Since donor doping should improve the time-dependent dielectric breakdown behavior [19], it may also allow larger fields to be applied without degrading the reliability. A PZT based series switch is shown schematically in Figure 24 below. Losses across switch contacts would be small in this

Figure 24. Series switch with stacked PZT layers
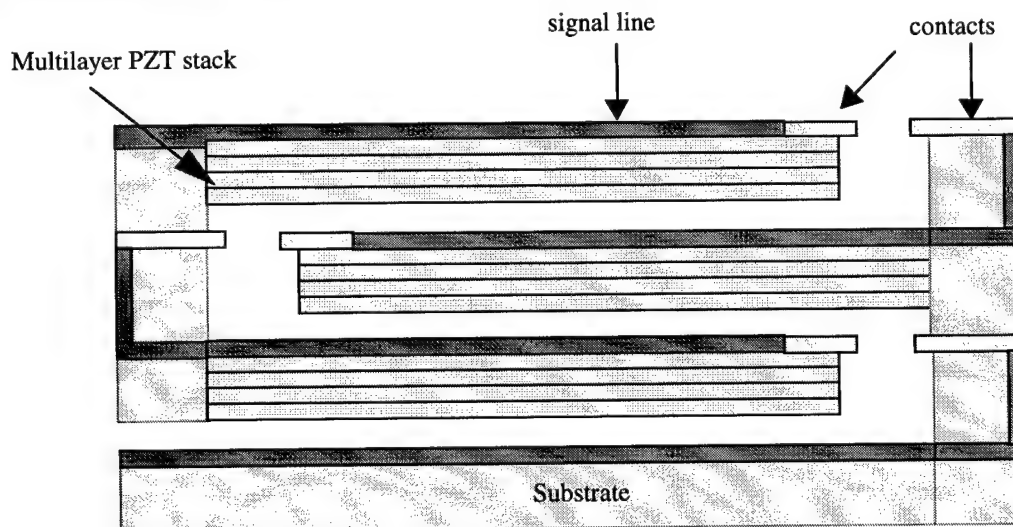
case because the closing forces are large.

Another approach would be to switch actuator materials to one that has inherently high strain. One of the possibilities being considered here is antiferroelectric phase switching compounds based on $PbZrO_3$. In this case, applied electric fields result in a field-forced antiferroelectric to ferroelectric phase transformation. Since the latter has a much higher volume, the result is essentially a bipolar strain state with strains of several tenths of a percent. Alternatively, we will pursue a <001> oriented rhombohedrally distorted relaxor ferroelectric – $PbTiO_3$ solid solution. As has been shown by Shrout and Park in bulk single crystals [20], this orientation shows a piezoelectric coefficient as large as 2500 pC/N and longitudinal strains of 1.7%. Trolier-McKinstry's group has shown that, when these materials are grown as epitaxial or oriented thin films, they also show enhanced piezoelectric coefficients relative to randomly oriented PZT films of the same thickness [21,22]. Consequently, $Pb(Yb_{1/2}Nb_{1/2})O_3$-$PbTiO_3$ will also be investigated as necessary.

One key point to recognize in all cases is that the higher breakdown strengths of films enable them to be driven much harder than bulk materials of the same composition. PZT films, for instance, typically show breakdown strengths on the order of 500 kV/cm to 1 MV/m. The result is that substantial strains can be achieved, even when the piezoelectric coefficients are modest.

One can easily calculate the resonance frequency f_L of a bar with one end free and the other end clamped for the case of longitudinal propagation. The result is

$$f_L = \frac{\sqrt{E/\rho}}{4L} = \frac{V_s}{4L},$$

(8)

where E is Young's modulus, ρ is mass density, L is the length of the bar, and V_s is the speed of sound. For a PZT thin film, V_s is 3694 m/s.

If one sets L = 100 μm, one obtains f_L = 9.2 MHz, which corresponds to a 10% to 90% rise time of about 36 ns. For a PZT bar unconstrained by a substrate and doped with donors, the displacement would be of the order of 0.6 μm, and with two opposing bars this would double to 1.2 μm. As noted above, a series of such PZT bars would be required to obtain the appropriate switch isolation. However, if one were to instead use compounds based on $PbZrO_3$, strains of the order of 1% or greater would be achieved. For 1% strain, the single bar and double bar displacements would be of the order of 1 and 2 μm, respectively. Because tip displacement scales as L and resonance frequency scales as L^{-1}, there is a direct trade-off between tip displacement and time constant. By doubling the bar length from L = 100 μm to L = 200 μm, the switch rise time increases to 72 ns, and the tip displacement values increase to 2 and 4 μm for the single and double bars, respectively. Alternatively, one could use simply supported bars for the switch as illustrated in Figure 25 below. This would double the resonance frequency, which would yield a rise time of 18 ns for a 100 μm bar.
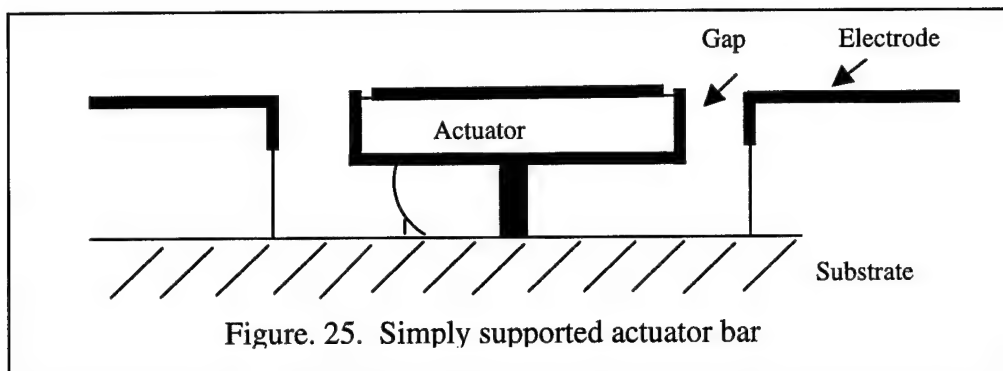
47

Figure. 25. Simply supported actuator bar

8.3 Flextensional Actuators

Flextensional transducers are mechanical amplifiers that couple longitudinal strains in ceramic bars and discs with a radial flexure of an oval metal shell. The concept of the flextensional transducer originated from the electroacoustic foghorn used for ship navigation in the early 1920's. A review of modern flextensional transducers may be found in [23]. Composite flextensional actuators (so-called moonies, rainbows, cymbals, and similar devices) [24-26] are of particular interest to this program because they can provide relatively large displacement (for good switch isolation) with relatively large stiffness and generative forces compared to simple bending actuators. Well-designed composite flextensional actuators can have an effective d_{33} many times larger than the piezoelectric material alone [25] and thus are intriguing candidates for miniaturization and integration as high-speed MEMS RF switches. However, the extent to which the resonance frequency is lowered by the flextensional structure is a key issue that must be addressed as part of the Phase 2 research program.
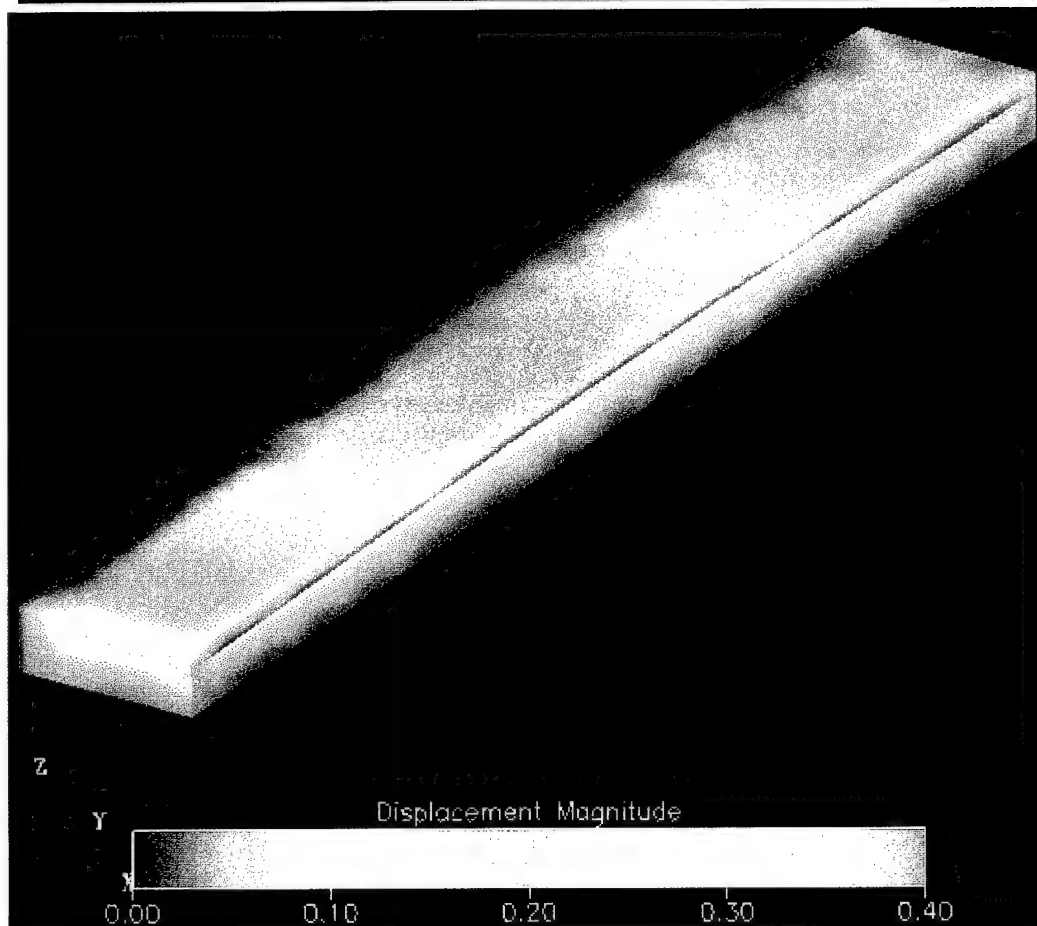
The so-called moonie is based on the principles of the flextensional transducer. A moonie consists of a piezoelectric ceramic element sandwiched between two metal end caps, each having a crescent shaped cavity on its inner surface. The metal end caps serve as mechanical transformers for converting and amplifying the lateral displacement of the ceramic into an axial motion normal to the caps. A detailed description of the design considerations for the moonie and cymbal actuators is provided in [27, 28].

Most of the previous research in the area of flextensional actuators has focussed on sensors made from bulk ceramics. It is of considerable interest to apply similar design strategies to MEMS switches. With the aid of MEMCAD we have modeled a simple arrangement wherein an aluminum cap has been added to a rectangular PZT beam. Views of the beam with and without the application of strain are shown in Figure 26. The PZT beam was chosen to be 150 μm (length) × 20 μm (width) × 5 μm (thickness) and the corresponding parameters for the aluminum cap were 150 μm × 20 μm × 2 μm. With no strain applied, the height of the center of the metal cap above the PZT was ~0.35 μm. With the application of -0.2% of strain to the PZT beam, the height of the metal cap increased to 1.40 μm. The conversion ratio between the transverse (inward) displacement of the PZT and the flexural displacement at the center of the metal cap is 3.5.

48

Figure 26 a.
Strain Applied

Displacement Magnitude

0.00   0.35   0.70   1.05   1.40

Figure 26 b.
No Strain

Displacement Magnitude

0.00   0.10   0.20   0.30   0.40

The lowest resonance frequency of the flextensional structure in Figure 26 can be roughly determined with the aid of expression (8). However, in this case E is the average value of Young's Modulus and ρ is the effective mass density of the system [17]. Detailed calculations have not yet been performed, but frequency estimates range between 3 and 6 MHz. Currently, we are in the process of resolving this uncertainty. The resonant frequency range corresponds to 10% to 90% rise times of ~100 ns to 50 ns. System designs incorporating flextensional structures appear to offer a means of enhancing displacement while preserving quick response times needed for switch closure.

We have examined the flextensional structure from the viewpoint of fabrication and have arrived at a preliminary methodology for its construction. This is illustrated in Figure 27. If a double cantilever were adopted as illustrated in Figure 28 (page 52), we would probably fabricate each cantilever separately and bond the two cantilevers at the anchor.

8.4 Combinations of Design Strategies

It may be to the advantage of the program to combine elements of the three design strategies offered above. For example, it may be advantageous for us to put a flextensional metal cap on the bottom of the bimorph cantilever (Section 8.1 above). This would offer a significant increase in signal isolation. The combination works because the bottom PZT layer in a bimorph must contract to drive the cantilever down. This inward contraction is exactly what is required to push the metal cap out. With this scenario, the bottom contact of the bimorph would actually retract when the switch is turned off and thereby provide added isolation.

Similarly, if it were determined to be feasible to develop actuator materials having higher strain, then the new material would redefine what could be done with flextensional and bimorph designs. For example, if the donor doping suggested for the extensional bar were implemented, it would favorably impact all design concepts.

8.5 Operating With Reverse Electric Field Polarization in PZT Thin Films

In general, one applies a static electric field to the PZT thin film in the same direction as it is polarized. This is done to prevent the PZT from depolarizing. In Phase 2, there may be a need to operate in a reverse polarization mode. In general, this is not a problem provided the imposed electric field is $\leq E_c$, the coercive electric field. Because E_c ~50 kV/cm, this limits the applied voltage to ~5 V across a 1 micron thin film. This level of reverse voltage is quite useful when one wants to control the overshoot of a cantilever as it is released from the closed switch position. One could apply a voltage waveform that is both positive (in the poling direction) and negative to bring the cantilever back to its static position smoothly.

The question arises as to whether larger reverse electric fields can be applied to the PZT thin film. One might want to do this for convenience when constructing a bimorph cantilever. With a bimorph cantilever, one would typically operate the upper PZT layer in d_{33} mode in the poling direction and the lower layer in the d_{31} mode, again in the poling direction. The reason for this is that when d_{33} is operated in the poling direction the PZT thin film expands, whereas when d_{31} is operated in the poling direction, it contracts. This occurs because the d_{31} piezoelectric coefficient is negative. However, one might want to simplify the fabrication process and use only d_{31} actuation. In this case, one would have to drive the PZT with an electric field opposite the poling direction at levels greater than ~50 kV/cm.

1. Silicon wafer with 2 μm sacrificial oxide layer
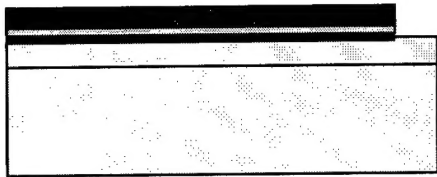
2. ZrO$_2$ is first spin coated and patterned. Metal electrode for d$_{33}$ mode operation is deposited by sputtering and patterned. Finally the PZT layer is deposited by sol-gel technique and fired. PZT is patterned into a cantilever shaped structure using ion-milling.
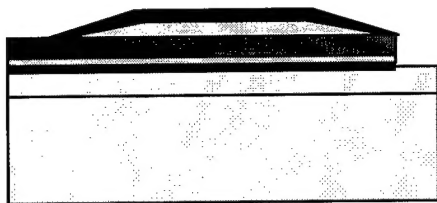
3. 1 mm polysilicon layer is deposited by LPCVD and patterned on top of the PZT cantilever on top of which a 1 μm gold layer is deposited and patterned.

4. A glass wafer is prepared by etching a 4 μm recess in it and metallized for signal lines.
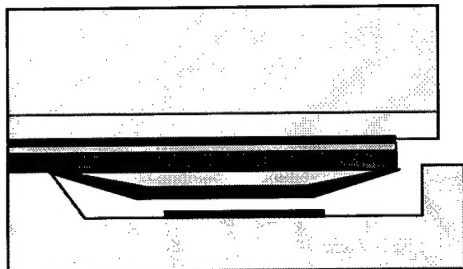
5. The glass wafer and the PZT coated silicon wafer are aligned and bonded together as shown.
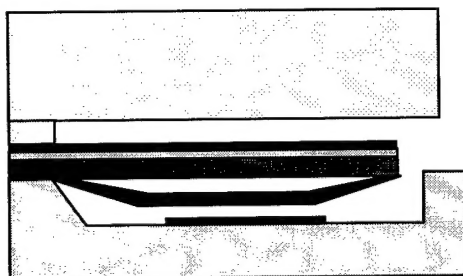
6. The sacrificial glass layer is etched under the PZT cantilever in HF. By controlling the aspect ratio of the structure, one can ensure that the cantilever is freestanding while the anchors are not etched away. Finally the polysilicon layer is dry etched in XeF$_2$ dry etchant so as to release the flextensional gold structure.

Figure 27. Fabrication of the flextensional cantilever

Figure 28.   Schematic illustration of two flextensional cantilevers with contacts facing one another.

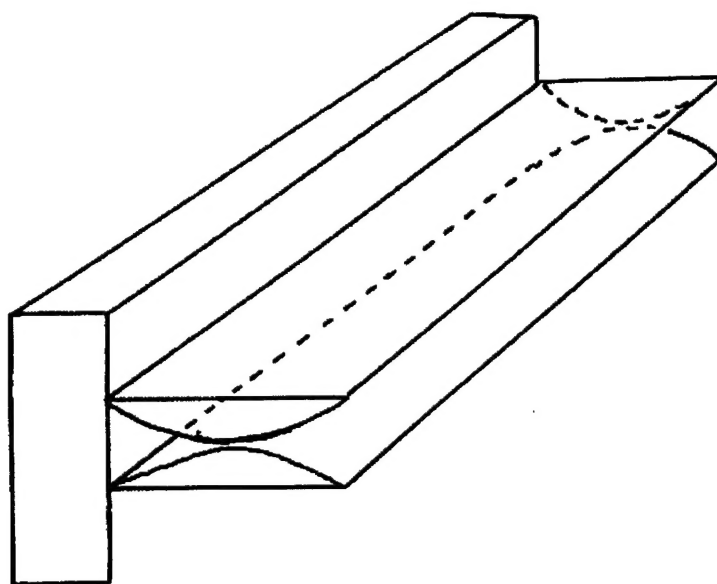There is at least one fabrication strategy that may be useful when applying large electric fields opposite to the polarization direction. This is to deliberately imprint the hysteresis loop as far as possible along the field axis. This may require us to move towards a vapor deposition method, because bombardment can be very effective here. Alternatively, we could attempt to put in very asymmetric electrodes, build in a strain gradient, align defect dipoles, or any combination of the above.

9. REFERENCES

[1]   Polla, D., Francis, L., "Processing and Characterization of Piezoelectric Materials and Integration into Microelectrical Systems," *Annual Review of Material Science 1998,* v. 28, pp. 563-597, 1998.

[2]   Polla, D., Francis, L., "Ferroelectric Thin Films in Microelectromechanical Systems Applications," *MRS Bulletin,* pp. 59-65, July 1996.

[3]   Wang, Q-M, and L. E. Cross, "Performance Analysis of Piezoelectric Cantilever Bending Acutuators," *Ferroelectrics*, v. 218, pp. 187-213, 1998.

[4]   Xu, Y., *Ferroelectric Materials and Their Applications*, Elsevier Science Publications, The Netherlands, 1998.

[5]   Polla, D., Francis, L., "Processing and Characterization of Piezoelectric Materials and Integration into Microelectrical Systems," *Annual Review of Material Science 1998,* v. 28, pp. 563-597, 1998.

[6]   Polla, D., Francis, L., "Ferroelectric Thin Films in Microelectromechanical Systems Applications," *MRS Bulletin,* pp. 59-65, July 1996.

[7]   Chen, H. D., K, R. Udayakumar, C. J. Gaskey, L. E. Cross, J. J. Bernstein, and L. C. Niles, "Fabrication and Electrical Properties of Lead Zirconate Titanate Thick Films," *J. Am. Ceram. Soc.,* 79, 2189-2192, 1996.

[8]   Chen, X., A. Kingon, K. Bellur, and O. Auciello, "DC Leakage and Failure of PZT Thin Film Capacitors for Non-Volatile Ferroelectric Memory and DRAM Applications," *Integ. Ferro.,* Vol. 5, pp. 59-72, 1994.

[9]   Waser R., T. Baiatu, and K-H. Hardtl, "Dc Electrical Degradation of Perovskite-Type Titanates: I, Ceramics," *J. Am. Ceram. Soc.,* Vol. 73, pp. 1645-53, 1990.

[10]   Waser, R. and M. Klee, "Theory of Conduction and Breakdown in Perovskite Thin Films," *Proc. 3rd Inter. Symp. Integ. Ferro.,* Colorado Springs, CO, 1991.

[11]   Raymond M. V., J. Chen, and D.M. Smyth, "Degradation of Ferroelectric Thin Films: A Defect Chemistry Approach," *Integ. Ferro.,* Vol. 5, pp. 73-8, 1994.

[12]   Lee, C., I. Toshihiro, and T. Suga, "Self-excited piezoelectric PZT microcantilevers for dynamic SFM - with inherent sensing and actuating capabilities," *Sensors and Actuators,* v. 72, no. 2, pp. 179-188, July 17, 1999.

[13]   Beck, C. M., M. M. Ahmed, C. J. Brierley, A. P. Needham, and S. P. Marsh, "Microwave Filters and Switches Produced Using Micro-Machining Techniques," *Proc. IMS 2000,* 31-36, 2000.

[14]   Djuth, F. T., T. S. Mayer, T. N. Jackson, S. Trolier-McKinstry, D. W. Machuga, and J. D. Mathews, "Low-Cost MEMS Switches for Military and Scientific Radars," in *Proc. of the Workshop on Affordability and Cost Reduction for Radar Systems 5-6 April, 2000,* U.S. Army Aviation and Missile Command Document SR-RD-MG-00-04, Huntsville, AL, 11 pp., 2000.

[15]   Lefki, K., and G. J. M. Dormans, *J. Appl. Phys.* 76, 1764 (1994).

[16]   Shaw, T. M., S. Trolier-McKinstry, and P.C. McIntyre, "The Properties of Ferroelectric Films at Small Dimensions," *Annu. Rev. Mater. Sci.,* 30, 263-298 (2000).

[17]   Zhang, X.L., Chen ZX, Cross LE, Schulze WA. 1983. *J. Mat. Sci.* 18: 968

[18]   Kholkin, A., "Non-linear piezoelectric response in lead zirconate-titanate (PZT) films," *Ferroelectrics,* 238: (1-4) 799-807 (2000).

[19]   Dimos, D., R. W. Schwartz, and S. J. Lockwood, "Control of Leakage Resistance in $Pb(Zr,Ti)O_3$ Thin Films by Donor Doping," *J. Am. Ceram. Soc.,* 77, 3000-30005 (1994).

[20]   Park, S. E., T. R. Shrout, "Relaxor based ferroelectric single crystals for electro-mechanical actuators," *Materials Research Innovations,* 1: (1) 20-25 (1997).

[21]   Maria, J-P, Ph.D. Thesis, the Pennsylvania State University (1998).

[22]   Yoshimura, T., and S. Trolier-McKinstry, "Transverse Piezoelectric Propertries of Epitaxial $Pb(Yb_{1/2}Nb_{1/2})O_3 - PbTiO_3$ (50/50) Films," accepted by *Thin Solid Films.* (2000).

[23]   Rolt, K. D., *J. Acoust. Soc. Am.,* 87, 1340-1345, 1990.

[24]   Newnham, R.E.; Dogan, A.; Xu, Q.C.; Onitsuka, K.; Tressler, J.; Yoshikawa, S., "Flextensional `moonie' actuators," *Proceedings of the IEEE 1993 Ultrasonics Symposium. Part 1 (of 2),* pp. 509-513, Oct 31-Nov 3 1993.

[25]   Shih, W.Y.; Shih, W.-H.; Aksay, I.A., "Scaling analysis for the axial displacement and pressure of flextensional transducers," *Journal of the American Ceramic Society,* v. 80, n 5, pp. 1073-1078, May 1997.

[26]   Butler, S. C, A. L. Butler, and J. L. Butler, Directional flextensional transducer, *J. Acoust. Soc. Am.,* 92, 2977-2979, 1992.

[27]   Xu, Q. C., A. Dogan, J. Tressler, S. Yoshikawa, and R. E. Newnham, "Ceramic-Metal Composite Actuator," *Proceedings of the IEEE 1991 Ultrasonics Symposium,* pp. 923-928, 1991.

[28]   Dogan, A, K. Uchino, and R. E. Newnham, "Composite piezoelectric transducer with truncated conical endcaps 'cymbal'," *IEEE Transactions on Ultrasonics, Ferroelectrics, and Frequency Control,* v. 44, n 3, pp. 597-605, May 1997.

[29]   Munikoti, R., and P. Dhar, "Highly Accelerated Life Testing (HALT) for Multilayer Ceramic Capacitor Qualification," *IEEE Trans. Comp. Hyb. Manu. Tech.,* Vol. 11, pp. 342 - 45, 1988.